(10) J. R. Schaefgen, T. I. Bair, J. W. Ballow, S. L. Kwolek, P. W. Morgan, M. Panar, and J. Zimmerman, "Ultra-High Modulus Polymers", A. Ciferri and I. M. Ward, Eds., Applied Science, London, 1979.
(11) L. L. Chapoy, D. Spaseska, K. Rasmussen, and D. B. DuPré, *Macromolecules*, **12**, 680 (1979).
(12) H. F. Mark, N. G. Gaylord, N. M. Bikales, Eds., "Encyclopedia of Polymer Science and Technology", J. Wiley and Sons, New York. Compare the following: L. Rebenfeld, "Fibers", Vol. 6, pp 505 ff, 1967.; H. F. Arledter, "Inorganic Fibers", Vol. 6, pp 610 ff, 1967; J. Preston, "Aromatic Polyamide Fibers", Suppl. Vol. 2, pp 84 ff, 1977.
(13) P. J. Flory, *Proc. R. Soc. London, Ser. A.* **234**, 73 (1956); *J. Polym. Sci.*, **49**, 105 (1961).
(14) P. W. Morgan, *J. Polym. Sci., Polym. Symp.*, **65**, 1 (1978).
(15) J. Preston, *Polym. Eng. Sci.*, **15**, 199 (1975).
(16) E. Bianchi, A. Ciferri, J. Preston, and W. R. Krigbaum, *J. Polym. Sci., Polym. Phys. Ed.*, **19**, 863 (1981).
(17) E. Bianchi, A. Ciferri, A. Tealdi, and W. R. Krigbaum, *J. Polym. Sci., Polym. Phys. Ed.*, **17**, 2091 (1979).
(18) G. Marucci and A. Ciferri, *J. Polym. Sci., Polym. Lett. Ed.*, **15**, 643 (1977).
(19) D. G. Baird, A. Ciferri, W. R. Krigbaum, and F. Salaris, *J. Polym. Sci., Polym. Phys. Ed.*, **17**, 1649 (1979).
(20) B. Valenti and A. Ciferri, *J. Polym. Sci., Polym. Lett. Ed.*, **16**, 657 (1978).
(21) L. L. Chapoy and N. F. la Cour, *Rheol. Acta*, **19**, 731 (1980).
(22) D. G. Baird and R. L. Ballman, *J. Rheol. (N.Y.)*, **23**, 505 (1979).
(23) S. G. Chu, S. Venkatraman, G. C. Berry, and Y. Einaga, *Macromolecules*, **14**, 939 (1981).
(24) D. G. Baird, presented at the IUPAC 28th Macromolecular Symposium, Amherst, MA, July 12–16, 1982.
(25) W. R. Krigbaum and S.Sasaki, *J. Polym. Sci., Polym. Phys. Ed.*, **19**, 1339 (1981).
(26) P. R. Dvornic, *J. Appl. Polym. Sci.*, **28**, 2729 (1983).
(27) W. W. Graessley, *J. Chem. Phys.*, **47**, 1942 (1967).
(28) W. W. Graessley and L. Segal, *Macromolecules*, **2**, 49 (1969).
(29) P. E. Rouse, *J. Chem. Phys.*, **21**, 1272 (1953).
(30) T. W. Dewitt, H. Markovitz, F. J. Padden, and L. J. Zapas, *J. Colloid Sci.*, **10**, 174 (1955); F. Bueche and S. W. Harding, *J. Polym. Sci.*, **32**, 177 (1958).
(31) Although it was proposed (J. Klein, *Macromolecules*, 11, 825 (1978)) to relate the onset of entangled behavior to the conditions at which molecular diffusion of polymer segments becomes restricted to reptation alone (For details on reptation model see ref 38–40.), it still seems that the precise nature of entanglements and their role are not very well understood as yet. One view envisions that an entanglement forms when two macromolecular chains tightly kink around each other by bending back on themselves in short-range contour, while another view holds that coupling involves only looping of chains around each other in their long-range contour. (W. W. Graessley, *J. Chem. Phys.*, **43**, 2696 (1965); S. F. Edwards, *Proc. Phys. Soc.*, **91**, 513 (1967).)
(32) M. Daoud, J. P. Cotton, B. Farnoux, G. Janninek, G. Sarma, H. Benoit, C. Duplessix, C. Picot, and P.-G. de Gennes, *Macromolecules*, **8**, 804 (1975).
(33) H. L. Frisch and R. Simha in "Rheology", F. R. Eirich, Ed., Academic Press, New York, 1956, Vol. I, Chapter 14.
(34) R. S. Porter and J. F. Johnson, *Chem. Rev.*, **66**, 1 (1966).
(35) G. C. Berry and T. G. Fox, *Adv. Polym. Sci.*, **5**, 261 (1968).
(36) W. W. Graessley, *Adv. Polym. Sci.*, **16**, 1 (1974).
(37) J. D. Ferry, "Viscoelastic Properties of Polymers", J. Wiley and Sons, New York, 1970.
(38) P.-G. de Gennes, *J. Chem. Phys.*, **55**, 572 (1971).
(39) M. Doi and S. F. Edwards, *J. Chem. Soc., Faraday Trans. 2*, **74**, 1789 (1978).
(40) M. Doi and S. F. Edwards, *J. Chem. Soc., Faraday Trans. 2*, **74**, 1802, 1818 (1978); **75**, 38 (1979).
(41) F. Bueche, *J. Chem. Phys.*, **20**, 1959 (1952).
(42) F. Bueche, "Physical Properties of Polymers", Interscience, New York, 1962.
(43) T. G. Fox and V. R. Allen, *Polymer*, **3**, 111 (1962).
(44) G. C. Berry, V. C. Long, and L. M. Hobbs, *J. Chem. Phys.*, **44**, 4550 (1966).
(45) C. W. Pyun and M. Fixman, *J. Chem. Phys.*, **42**, 3838 (1965).
(46) The same value was earlier reported (ref 25) to equal 0.682 cm^3/g at 23 °C as determined by density measurements.
(47) T. G. Fox and V. R. Allen, *J. Chem. Phys.*, **41**, 344 (1965).
(48) S. M. Aharoni, *J. Appl. Polym. Sci.*, **21**, 1323 (1977).
(49) D. W. van Krevelen and P. J. Hoftyzer, *J. Appl. Polym. Sci.*, **10**, 1331 (1966).
(50) F. Millich, E. W. Hellmuth, and S. Y. Huang, *J. Polym. Sci., Polym. Chem. Ed.*, **13**, 2143 (1975).
(51) S. Y. Huang and E. W. Hellmuth, *Polym. Prepr., Am. Chem. Soc., Div. Polym. Chem.*, **15**(1), 499, 505 (1974).
(52) S. M. Aharoni, *Polym. Prepr., Am. Chem. Soc., Div. Polym. Chem.*, **23**(1), 275 (1982).
(53) J. J. Burke, *J. Macromol. Sci., Chem.*, **A7**(1), 187 (1973).

Unified Description of Temperature and Concentration Crossover in the Excluded Volume Problem. 1. Osmotic Pressure and Correlation Lengths

Lothar Schäfer*

Institut für Theoretische Physik der Universität Hannover, 3000 Hannover, Federal Republic of Germany. *Received June 17, 1983*

ABSTRACT: We use renormalization group theory to calculate all experimentally accessible correlation lengths and thermodynamic quantities for a dilute polymer solution. Our calculation covers the whole universal regime above the Θ-temperature ranging from single-chain to semidilute limits. Omitting the details of the calculations, we concentrate on the basic features of the method, and we carefully discuss the crossover diagram. Results of a consistent first-order calculation for all the above-mentioned quantities are given and are compared to experiment. In general, the agreement is very good. Discrepancies that occur in the semidilute Θ-limit are analyzed.

1. Introduction

Dilute solutions of long-chain molecules show two different types of crossover phenomena. In pure form the first type is observed if we increase the temperature T of a very dilute solution (i.e., number concentration c_p of chains almost zero) above the Θ-temperature. At $T = \Theta$ the effective interaction $\beta(T)$ of any two chain segments vanishes and therefore the long-range correlations within one chain are Gaussian. The radius of gyration R_g obeys a simple random walk law $R_g \sim N^{1/2}$ as a function of the number of monomers per chain N. Increasing T such that $\beta(T)N^{1/2} >> 1$, we reach the excluded volume limit. Here the long-range properties of the chains are dominated by the repulsive interaction $\beta(T)$. The correlations are non-

* Permanent address: Universität Essen, Fachbereich 7-Physik, 4300 Essen 1, Federal Republic of Germany.

0024-9297/84/2217-1357$01.50/0

trivial and the radius of gyration of an isolated chain behaves as $R_g \sim N^\nu$, $\nu \cong {}^3/_5$. Much experimental and theoretical work has aimed at an understanding of the crossover between the Θ-limit and the excluded volume limit. A review of earlier work can be found in the book of Yamakawa.[1]

The second crossover takes us from the dilute limit, where a virial expansion holds, to the semidilute limit $l^3c_pN << 1$, $\beta(T)R_g^3c_p >> 1$ (l denotes a microscopic length of the order of the size of a monomer), where the chains overlap and interact strongly. In this limit the virial expansion breaks down. Collective effects due to the interaction of many chains become dominant.[2] The crossover in concentration between these two limits has been discussed only recently,[3] this work being restricted to thermodynamic quantities in the excluded volume limit. Other recent work[40,41] on this crossover ignores some specific features of the collective effects in the semidilute limit (see the discussion below eq 2.29).

Much of the recent interest in these problems arises from the observation that the long-range behavior of polymer solutions in the region $T \geq \Theta$, $N >> 1$, $l^3c_pN << 1$ is universal, which means that it is the same for a large class of chemically different solutions. The chemical microstructure only influences a few nonuniversal scale factors. This suggests that a general theory ignoring complications of microstructure can be found, and indeed such a theory is established by the renormalization group. Within this approach various properties of the dilute excluded volume limit have been calculated. The temperature crossover in the dilute limit has also been discussed extensively.[4-6] Some work on the semidilute limit has been done,[7,8] and—as mentioned above—the concentration crossover in the excluded volume limit has been analyzed. Furthermore, the entropy of the solution has been calculated in the whole critical regime.[9]

The renormalization group is a well-defined concept which, however, allows for a number of realizations that differ in technical details. Since all calculations of crossover functions are restricted to low order in some kind of perturbation theory, these technical differences influence the numerical results. The choice of the realization is largely a matter of taste, and for a given physical quantity often most of the numerical difference in the results can be absorbed into an adjustment of the nonuniversal scale factors. Still we feel that the experimental and theoretical situation asks for a consistent calculation of *all* accessible physical quantities within a *single* calculational scheme, and this calculation should cover the *full universal regime*. We have carried through such a calculation in the lowest nontrivial approximation, and here we report our results for the thermodynamic quantities and the correlation lengths. The momentum dependence of the correlation functions will be discussed in a second paper. Details of the calculations are lengthy and will not be reproduced here. Instead we concentrate on the basic philosophy of our method, stressing those aspects that are essential for a simultaneous treatment of both crossovers. The second major purpose of this paper is a comparison to experimental data in the whole critical regime. This shall clarify to what extent a low-order renormalization group calculation can give a consistent overall explanation of the experimental results.

The organization of the paper is as follows. In section 2 we present the basic structure of the theory. In section 3 we analyze the relation between the physical variables c_p, N, and T and the variables of the renormalized theory, and we discuss the relation between our crossover diagram and that of Daoud and Jannink.[10] The results for the correlation lengths and the thermodynamic scaling function are presented in section 4. In section 5 we analyze experiments in the whole critical region, and section 6 contains our conclusions.

2. Structure of the Theory

We use the well-known Gaussian model with excluded volume interaction. (Details of our conventions can be found in ref 11.) In this model the microstructure of the chains is characterized by the length l which gives the mean size of a Gaussian "monomer" and by the volume βl^3 which represents the strength of the two-body interaction in the cluster expansion. Globally the solution is characterized by the number concentration of polymer chains c_p and the (normalized) chain length distribution $P(n)$. The number-averaged chain length N is defined as

$$N = \sum_{n=1}^{\infty} nP(n) \tag{2.1}$$

We find it useful to introduce a reduced chain length distribution $p(x)$ together with its Laplace transform $\tilde{p}(y)$

$$P(n) = \frac{1}{N}p\left(\frac{n}{N}\right) \tag{2.2}$$

$$\tilde{p}(y) = \int_0^\infty \mathrm{d}x\ e^{-xy}p(x) \tag{2.3}$$

In replacing the summation over n by an integration over x in eq 2.3 we neglect terms of order $1/N$. The full effective Hamiltonian of the system contains terms in which more than two monomers interact simultaneously. In our calculations we have neglected these many-body interactions. They yield corrections in a neighborhood of the Θ-point which have been discussed in detail by Duplantier.[12] It will turn out that in the interpretation of some experiments, consideration of these many-body interactions is necessary.

The model we have described is specified by the parameters c_p, N, $p(x)$, β, and l. Each physical quantity can be calculated by expanding it in powers of β (cluster expansion). For large N the kth term of this expansion diverges as $(\beta N^{1/2})^k$ and we therefore need additional insight to set up a theory valid outside the Θ-region $\beta N^{1/2} << 1$. (We recall that $\beta(T = \Theta) = 0$ defines the Θ-point.)

The renormalization group (RG) provides that insight. In the language of polymer physics the basic idea is explained simply: Universal macroscopic properties of the system cannot depend on our choice of the microscopic degrees of freedom. Thus we should be able to describe our system by microscopic units of mean size l/λ instead of l. We have to admit that the new description needs new parameters $N(\lambda)$ and $\beta(\lambda)$, whereas the parameters c_p and $p(x)$ should not change. (This is the reason for introducing $p(x)$ in the place of $P(n)$.) For $\beta N^{1/2} >> 1$ the functions $N(\lambda)$ and $\beta(\lambda)$ cannot be calculated directly. It turns out, however, that the logarithmic derivatives of these functions can be calculated perturbatively even in the limit $N \to \infty$. The structure of the dilatation group $l \to l/\lambda$ then guarantees the existence of first-order differential equations

$$\frac{\mathrm{d}\ln\beta(\lambda)}{\mathrm{d}\ln\lambda} = \tilde{w}(\beta(\lambda))\left[1 + \mathcal{O}\left(\frac{1}{N}\right)\right] \tag{2.4}$$

$$\frac{\mathrm{d}\ln N(\lambda)}{\mathrm{d}\ln\lambda} = \tilde{v}(\beta(\lambda))\left[1 + \mathcal{O}\left(\frac{1}{N}\right)\right] \tag{2.5}$$

which can be integrated to find the desired results for $N(\lambda)$ and $\beta(\lambda)$. Knowledge of these functions allows us to map the system (c_p, $N >> 1$, $p(x)$, β, l) onto the system (c_p, $N(\lambda)$

~ 1, $p(x)$, $\beta(\lambda)$, l/λ). The function $\beta(\lambda)$ is found to be bounded by some "fixed-point" value β^*. As a result the variable $\beta N^{1/2} >> 1$ is mapped upon $\beta(\lambda)N(\lambda)^{1/2} \sim \beta^*$, and with this new variable the terms of the cluster expansion stay finite also for $N \to \infty$. The singularities that are characteristic of the excluded volume limit occur as properties of the mapping $N, \beta, l \to N(\lambda), \beta(\lambda), l/\lambda$.

The validity to all orders of perturbation theory of such a scheme has been proven in quantum field theory (see ref 13 for an introduction), and a special quantum field theory is intimately related to the polymer problem.[14] Consequently one can show that the RG works to all orders in the cluster expansion for the polymer system, even including such special features as polydispersity.[11] Once the general validity is proven, we can choose among numerous realizations of the basic ideas. We here use the "massless renormalization scheme" of field theory,[13] which allows us to exploit results extablished in the field theoretic context.[45]

In this method the parameters β and N are replaced by renormalized counterparts g and N_R. We write g as

$$g = g^* f \tag{2.6}$$

thus extracting the fixed-point value g^*. Under a change of the length scale $l \to l/\lambda$, the normalized coupling $f = f(\lambda)$ changes according to the implicit equation[15] (see also ref 4; in that reference, $\omega \cdot \nu$ is called ω).

$$\lambda = \left(\frac{1-f}{1-f_0}\right)^{1/\omega}\left(\frac{f}{f_0}\right)^{-1/\epsilon} \tag{2.7}$$

Here, $f_0 = f(\lambda = 1)$ is the initial value used in integrating the RG equation. It is assumed to be an analytic function of β. The critical exponent ω is positive, and $\epsilon = 4 - d$ is kept here to remind us that such relations are constructed by formally expanding about a $(d = 4)$-dimensional system. An equation similar to (2.7) relates N_R to N.

$$N_R = \left(\frac{1-f}{1-f_0}\right)^{1/\nu\omega}\left(\frac{f}{f_0}\right)^{-2/\epsilon} S_0(f_0)N \tag{2.8}$$

Here, $\nu > {}^1/_2$ denotes another critical exponent and $S_0(f_0)$ is assumed to be an analytic function of f_0 taking some finite positive value for $f_0 = 0$. Via the f dependence N_R implicitly is a function of λ. Equations 2.7 and 2.8 result from solving the RG equations (2.4) and (2.5), using expressions for $\tilde{w}(f)$ and $\tilde{\nu}(f)$ correct in order ϵ^2. (The difference of eq 2.8 compared to eq 2.19 in the second paper of ref 4 is due to a difference in notation. In that paper the variable $\tilde{N}$ denotes a "surface" $\tilde{N} \sim Nl^2$ in the sense of des Cloizeaux.[5]) Equations 2.7 and 2.8 define the mapping of f and N_R under the RG. We still have to consider the mapping for the physical quantities of interest. All thermodynamic quantities can be constructed[11] from the thermodynamic scaling function $\mathcal{P}$,[3] which is defined in terms of the osmotic pressure.

$$\frac{\Pi}{k_B T c_p} = 1 + \mathcal{P}(l^d c_p, N, f_0, p(x)) \tag{2.9}$$

Dimensional analysis guarantees that $\mathcal{P}$ depends on c_p and l only via the combination $l^d c_p$. The RG yields

$$\mathcal{P}(l^d c_p, N, f_0, p(x)) = \mathcal{P}(\lambda^{-d} l^d c_p, N_R(\lambda), f(\lambda), p(x)) \tag{2.10}$$

The other quantities considered in this paper are the correlation lengths. As a typical example we discuss the squared radius of gyration. Dimensional analysis yields

$$R_g^2(c_p, N, f_0, p(x), l) = l^2 \mathcal{R}(l^d c_p, N, f_0, p(x)) \tag{2.11}$$

Under the RG this transforms into

$$R_g^2(c_p, N, f_0, p(x), l) = \lambda^{-2} l^2 \mathcal{R}(\lambda^{-d} l^d c_p, N_R(\lambda), f(\lambda), p(x)) \tag{2.12}$$

As is well-known these results contain the scaling laws. To extract these laws we fix λ by imposing the condition

$$N_R(\lambda) = 1 \tag{2.13}$$

For $f_0 > 0$, $N \to \infty$ (excluded volume limit), eq 2.8 yields

$$(1 - f)^{1/\omega} \sim N^{-\nu} \to 0 \tag{2.14}$$

Thus $f \to 1$ and $\lambda \sim N^{-\nu} \to 0$. Substituting these results into eq 2.10 or 2.12, we find the scaling laws in the excluded volume limit. For example, the thermodynamic scaling function takes the form

$$\mathcal{P}(l^d c_p, N, f_0, p(x)) = \mathcal{P}(\text{const} \cdot N^{\nu d} l^d c_p, p(x)) \tag{2.15}$$

The Θ-limit is reached if f tends to zero, which implies $\lambda = (f/f_0)^{-1/\epsilon}$ and $N^{-1} = (f_0/f)^{2/\epsilon} S_0(f_0)$. Taking N fixed, we see that f_0 tends to zero together with f.

$$f = f_0 (S_0(0)N)^{\epsilon/2} \tag{2.16}$$

Substituting this, for instance, into the expression for R_g^2, we find the well-known result

$$R_g^2 = S_0(0) N l^2 \mathcal{R}(S_0(0)^{d/2} N^{d/2} l^d c_p, f_0 (S_0(0)N)^{\epsilon/2}, p(x)) \tag{2.17}$$

valid in the Θ-limit.

Equations 2.7 and 2.13 contain the full temperature crossover in the dilute limit. Obviously, for $c_p \to 0$ a virial expansion exists for any quantity of interest, and the coefficients of such an expansion up to some power of λ are just functions of $N_R(\lambda)$, $f(\lambda)$, and $p(x)$. With $N_R(\lambda) = 1$ we can calculate these coefficients as functionals of $p(x)$ in a well-behaved renormalized perturbation expansion in powers of $f(\lambda)$. Elderfield[4] was the first to calculate in this way the temperature crossover for virial coefficients of the osmotic pressure and for the radius of an isolated chain.

Whereas the temperature crossover is adequately dealt with by the RG, this method alone is not sufficient to understand the concentration crossover. Indeed, reconsidering, for example, eq 2.15, which exploits the full power of the RG in the excluded volume limit, we find that the scaling function $\mathcal{P}$ depends on $N^{\nu d} c_p$, which diverges in the semidilute limit Nc_p fixed, $N \to \infty$. (Note that $\nu \cong {}^3/_5$ for $d = 3$.) As a consequence all coefficients in the formal Taylor series for $\mathcal{P}$ in powers of f diverge in the semidilute limit, and the degree of divergence increases with increasing order in perturbation theory. To solve this problem we have to exploit the screening effect, which in this context was first discussed by Edwards.[2] Reordering the cluster expansion in the Θ-region he constructed a momentum-dependent effective interaction which in the semidilute limit vanishes rapidly for inverse momenta q^{-1} larger than some "screening length" ξ. This length depends on the monomer concentration

$$c_1 = c_p N \tag{2.18}$$

but is otherwise independent of N. In the semidilute limit R_g is large compared to ξ, and since the effective interaction on the scale $R_g >> \xi$ vanishes, the correlations on that scale are Gaussian. Results like $R_g \sim r(c_1)N^{1/2}$ follow. Assuming that the screening mechanism works also in the semidilute excluded volume limit and combining it with the scaling laws, de Gennes[16] and co-workers developed the "blob model", which qualitatively explains the experimental results.

We now incorporate these ideas into the RG approach. It will help the understanding to note the mean field re-

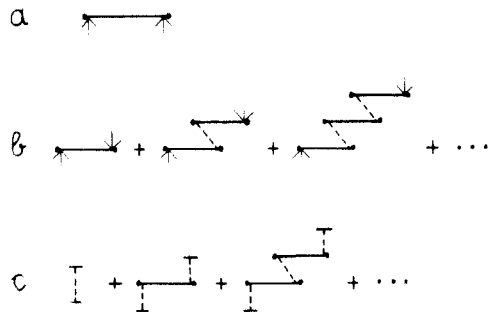

Figure 1. (a) Diagrammatic representation of the density autocorrelation function $I_a(q)$ in mean field approximation. (b) Diagrams summed to get $I_c(q)$. (c) Diagrams contributing to the screened interaction.

sults for R_g and ξ. R_g is defined in terms of the density autocorrelation function $I_a(q)$, which in mean field theory essentially coincides with the Debye function

$$I_a(q)/c_1N = 2Q^{-4}(\tilde{p}(Q^2) + Q^2 - 1) = \tilde{p}'' + \tfrac{1}{3}\tilde{p}'''Q^2 + \mathcal{O}(Q^4) \quad (2.19)$$

Here

$$Q = qlN_R^{1/2}\lambda^{-1} \quad (2.20)$$

is the renormalized momentum transfer. Equations 2.19 and 2.20 yield

$$R_g^2 = -\mathrm{d}\frac{\partial}{\partial q^2} \ln I_a(q) = -\frac{d}{3}\frac{\tilde{p}'''}{\tilde{p}''}l^2\lambda^{-2}N_R(\lambda) \quad (2.21)$$

To define ξ we note that for distances large compared to this screening length the monomers should feel no nontrivial correlation. It therefore is reasonable to identify ξ with the density correlation length which is derived from the density correlation function $I_c(q)$ for monomers on arbitrary chains. In mean field theory this function is found by summing all simply connected sequences of polymer chains (Figure 1b). In renormalized variables the result takes the form

$$\frac{c_1N}{I_c(q)} = \frac{c_1N}{I_a(q)} + gl^dc_p\lambda^{-d}N_R^2(\lambda) \quad (2.22)$$

The expression

$$\xi^2 = -\mathrm{d}\frac{\partial}{\partial q^2} \ln I_c(q) = \frac{R_g^2}{1 + gl^dc_p\tilde{p}''\lambda^{-d}N_R^2(\lambda)} \quad (2.23)$$

follows. It is easily checked that in the semidilute Θ-limit ξ^2 stays finite for finite c_1, independent of N: $\xi^2 \sim (f_0c_1)^{-1}$.

The renormalization condition $N_R(\lambda) = 1$ implies that we dilate the microscopic length scale l until it essentially coincides with R_g: $R_g \sim l/\lambda$. The RG is a way to treat a strongly interacting system, but according to the screening hypothesis, the system does not interact on the scale R_g. It is therefore not reasonable to carry the RG to $\lambda \sim l/R_g$. Rather, we should fix λ by imposing the condition $\xi \sim l/\lambda$. With eq 2.21 and 2.23, this yields

$$1 = \frac{1}{N_R(\lambda)} + gc_{1R}(\lambda) \quad (2.24)$$

where we omitted some unimportant constants and introduced

$$c_{1R}(x) = l^dc_p\lambda^{-d}N_R(\lambda) = l^dc_1\left(\frac{1-f}{1-f_0}\right)^{(1/\nu\omega)(1-\nu d)}\left(\frac{f}{f_0}\right)^{(2-\epsilon)/\epsilon}S_0(f_0) \quad (2.25)$$

In the dilute limit, eq 2.24 and 2.13 coincide. In the semidilute limit, however, eq 2.24 fixes f, and thus λ, as a function of c_1 independent of N, and $N_R(\lambda)$ is found to diverge proportional to N. All the results of the blob model follow. This discussion does not ensure that the renormalized theory together with eq 2.24 provides a consistent calculational scheme. Indeed we just shifted the divergence from the variable $\lambda^{-d}l^dc_p$ to the variable $N_R(\lambda)$, and clearly, higher orders in perturbation theory now can exhibit singular powers of N_R. We have to look more closely into the screening effect to show that these singularities are suppressed. In mean field theory the screened interaction $g(q)$ is found by the same summation of sequences of chains that gives $I_c(q)$. The diagrams of Figure 1c yield

$$g(q) = g\frac{I_c(q)}{I_a(q)} \quad (2.26)$$

In the dilute limit we have $I_c(q) \cong I_a(q)$ and thus $g(q) \cong g$. In the semidilute limit we find

$$g(q) \cong g\left[1 + \frac{R_g^2}{\xi^2}\frac{I_a(q)}{c_1N}\right]^{-1} \quad (2.27)$$

For $Q^2 \cong q^2R_g^2 >> 1$ we can approximate $I_a(q) \cong 2c_1NQ^{-2}$, which yields

$$g(q) \cong g\left[1 + 2(q\xi)^{-2}\left(-\frac{d}{3}\frac{\tilde{p}'''}{\tilde{p}''}\right)\right]^{-1} \quad (2.28)$$

For $q\xi \gtrsim 1$ the effective interaction is of order g, but it decreases rapidly as $q\xi$ decreases:

$$g(q) \sim g(q\xi)^2 \qquad \text{for } \xi^{-2} >> q^2 >> R_g^{-2} \quad (2.29a)$$

For $q \to 0$ it tends to

$$g(0) \cong \frac{1}{N_R}(\tilde{p}''^2c_{1R})^{-1} \quad (2.29b)$$

Dimensional analysis suggests that the leading singularity of the kth order of the cluster expansion takes the form $(g(0)N_R^{\epsilon/2})^k \sim N_R^{k(\epsilon/2-1)}$, which shows that the screening effect is able to suppress the singularities.

This rough discussion has presented the essential ideas necessary for a treatment of the concentration crossover. Much more work is necessary to show that this allows for consistent calculations. Details can be found in ref 17, where the same problem has been considered in the context of phase transitions. The result is that a meaningful calculation can be done in the framework of a double expansion in ϵ (note that $g = g^*f = \mathcal{O}(\epsilon)$) and $(N_R^{\epsilon/2} - 1)/N_R$. The latter parameter governs the corrections to the semidilute limit and it *should not be expanded* in powers of ϵ: It incorporates the structure of the screening effect, and this is independent of renormalization group and ϵ-expansion. Due to this double expansion, explicit results in the semidilute region typically take the form

$$A(N,c_p)_{\hat{s}\to\infty} = N^\alpha\hat{s}^\beta[a_1(\epsilon) + a_2(\epsilon)\hat{s}^{-1/(\nu d-1)}(\hat{s}^{\epsilon/2(\nu d-1)} - 1) + a_3(\epsilon)\hat{s}^{-1/(\nu d-1)} + ...] \quad (2.30)$$

$$\hat{s} \sim c_1N^{\nu d-1}$$

where the exponents α and β and the coefficients $a_i(\epsilon)$ depend on the quantity A under consideration. This structure can simply be checked, for instance, by expanding R_g^2 (eq 4.27) for large overlap. The simpler approach of ref 40 and 41 ignores the role of the second expansion parameter, thus approximating

$$\hat{s}^{\epsilon/2(\nu d-1)} - 1 \cong \frac{\epsilon}{2}\ln\hat{s}$$

Whereas for some quantities this may be a numerically acceptable approximation, it clearly loses the full structure of the screening mechanism. As a very important technical aspect we finally note that in higher orders we have to modify the definition of the screened interaction in order to preserve the screening effect.

In the following sections we present some results of our calculations. In contrast to other work,[5,6] we expand only the scaling functions like $\mathcal{P}$ and $\mathcal{R}$ in eq 2.10 or 2.13, but we keep the best known values of the exponents

$$\nu = 0.588$$
$$\omega = 0.790 \qquad \text{for } d = 3 \tag{2.31}$$

(In fact we only expand "one-vertex-irreducible" substructures of scaling functions. This explains why some of our results are not ordered strictly in powers of ϵ or $(N_R^{\epsilon/2} - 1)/N_R$.)

The RG equations (2.7) and (2.8) guarantee that the Θ-limit and the excluded volume limit are described correctly, and the choice (2.24) of λ together with the double expansion yields the correct description of the semidilute and the dilute limits. In our view all these features are essential for a meaningful comparison to experiment.

3. Crossover Diagram

In our explicit calculations we found it convenient to replace condition (2.24) by

$$1 = w + 2g(c_{lR} - c) \tag{3.1}$$

where

$$gc = \frac{\epsilon}{16} f(1 - w) + \frac{f}{8} w(w^{-\epsilon/2} - 1) \tag{3.2}$$

and

$$w = N_R^{-1}\left(1 - \frac{c}{c_{lR}}\right)^{-1} \tag{3.3}$$

This modification is within the range allowed by the general considerations. Equations 3.1, 3.3, and 2.8 yield

$$\frac{w}{1 + 2gc/(1 - w)} = N_R^{-1} = (1 - f)^{-1/\nu\omega} f^{2/\epsilon} \hat{N}^{-1} \tag{3.4}$$

where

$$\hat{N} = s_N N \tag{3.5}$$

$$s_N = s_N(f_0) = (1 - f_0)^{-1/\nu\omega} f_0^{2/\epsilon} S_0(f_0) \tag{3.6}$$

Equations 3.1 and 2.25 yield

$$1 - w + 2gc = 2gc_{lR} = 2f^{2/\epsilon}(1 - f)^{(1-\nu d)/\nu\omega} \hat{c}_l \tag{3.7}$$

where

$$\hat{c}_l = g^* s_N s_l^d c_l \tag{3.8}$$

$$s_l = s_l(f_0) = (1 - f_0)^{1/\omega} f_0^{-1/\epsilon} l \tag{3.9}$$

Equations 3.4 to 3.9 constitute the mapping from unrenormalized variables $f_0(T)$, c_l, and N to renormalized "scaling fields" w and f. All the f_0 dependence is contained in two nonuniversal scale functions $s_N(f_0)$ and $s_l(f_0)$. Once the values of these functions are fixed, the (c_l, N) dependence is universal. All scaling functions can be expressed in terms of w and f.

The scaling fields w and f are useful intermediate variables which cannot be measured directly; indeed they depend on technical features of the method, which is the source of the apparent differences among the results found in the literature. However, in mean field theory they allow for a simple physical interpretation. Up to higher order terms, f is proportional to the interpenetration function (see section 4.2) whereas w determines the ratio of ξ to R_g.

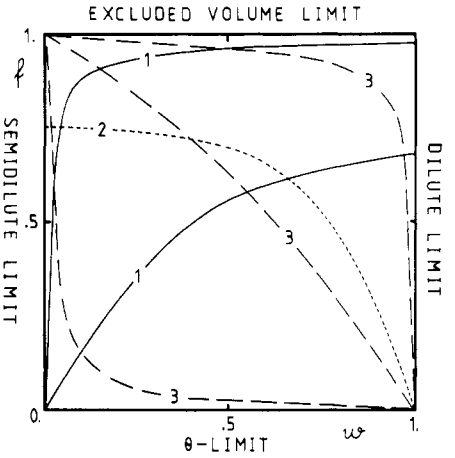

Figure 2. Crossover diagram in terms of nonlinear scaling fields w,f. The lines correspond to the following. Type 1: N and T fixed, c_l varies; type 2: c_l and T fixed, N varies; type 3: c_l and N fixed, T varies.

$$\frac{\xi^2}{R_g^2} = (1 + gN_R c_{lR} \tilde{p}'')^{-1}(1 + \mathcal{O}(f)) = \frac{w}{w + (1 - w)p''/2}(1 + \mathcal{O}(f)) \tag{3.10}$$

w tends to one in the dilute limit and approaches zero in the semidilute limit; $f \to 0$ or $f \to 1$ defines the Θ-limit or the excluded volume limit, respectively.

Any experiment traces out a path in the w–f diagram (Figure 2), and we distinguish three typical cases. Measuring some quantity as a function of c_l for fixed N and T, we follow a path of type 1. Note that with increasing c_l (i.e., decreasing w) the screening effect becomes more effective. Thus f decreases, and eventually all such paths reach the semidilute Θ-limit $f = w = 0$. A path starting at $w = 1$ close to $f = 1$ almost reaches the semidilute excluded volume limit $w = 0, f = 1$ and bends sharply from excluded volume to semidilute behavior. As a consequence, in the experiments we expect to see a double crossover as a function of c_l: First there is the concentration crossover $(w = 1) \to (w \cong 0)$ in the excluced volume regime $f \cong 1$ which then is followed by the semidilute $(w \cong 0)$ "temperature" crossover $(f \cong 1) \to (f = 0)$. Figure 4 gives an example of such a behavior.

The second type of experiments consists in changing N for fixed c_l and T. The corresponding paths (type 2 in Figure 2) all start at $f = 0, w = 1$ and end at the semidilute line $w = 0$ (provided $c_l \neq 0$).

In experiments of the third type we change T for fixed c_l and N. To find the corresponding paths we need to know the functions $s_N(f_0(T))$ and $s_l(f_0(T))$. These paths therefore are not universal. Universality in the sense of the standard two-parameter theories is recovered for temperatures near Θ: $(T - \Theta)/\Theta << 1$ where $f_0(T) << 1$. In this region the parametrizations

$$\hat{f}_0 = S_0^{\epsilon/2}(f_0) f_0 = u\frac{T - \Theta}{\Theta} \tag{3.11}$$

$$\hat{l} = l S_0^{1/2}(f_0) = \text{constant} \tag{3.12}$$

are justified theoretically. Empirically, these approximations often hold in all the accessible temperature range.

We may argue that $f_0 << 1$ is a necessary requirement for the very observation of the temperature crossover.

Taking a value $f_0 \sim 0.1$ as an upper limit of the two-parameter regime, from eq 3.5 and 3.6 together with $S_0(0) \cong 1$ we find $\hat{N} \cong 0.01N$. The universal regime is restricted to long chains; $N \gtrsim 500$ seems to be a reasonable requirement. Using the corresponding value $\hat{N} = 5$ in eq 3.4, we find that values $f \lesssim 0.7$ correspond to the two-parameter regime in the dilute limit. For longer chains this bound increases. Thus in general a large part of the temperature crossover can be tested only within the range of the two-parameter theory. Clearly, this rough estimate cannot rule out exceptions due to specific microstructure effects. It, however, is consistent with the parameter values found in our analysis of experiments.

In three dimensions ($\epsilon = 1$) the two-parameter assumption yields the scale functions

$$s_N = \hat{f}_0^2 \tag{3.13}$$

$$s_l = \hat{f}_0^{-1}\hat{l} \tag{3.14}$$

Changing T, we therefore go along a path of fixed

$$\hat{c}_1\hat{N}^{1/2} = g^*\hat{l}^3 c_1 N^{1/2} \tag{3.15}$$

All these paths start at the dilute Θ-limit $f = 0$, $w = 1$. This holds independently of the *geometrical* overlap $c_p R_g^3$. It is the *dynamical* overlap $\hat{f}_0 N^{1/2} c_p R_g^3$ that governs w in the Θ-region. With increasing temperature, f increases, and at the same time screening becomes effective. All paths end at the semidilute excluded volume limit $f = 1$, $w = 0$. Three typical paths are given in the f–w diagram of Figure 2. In extreme cases $\hat{c}_1\hat{N}^{1/2} << 1$ or $\hat{c}_1\hat{N}^{1/2} >> 1$ we again expect to observe double-crossover phenomena.

The scaling behavior resulting from the two-parameter assumption is well-known, and a schematic crossover diagram identifying the different limiting regions was first published by Daoud and Jannink[10] (see also ref 18). Having established an explicit form of the mapping between renormalized and unrenormalized variables, we can give a more quantitative form of their diagram. We define the limiting regions such that the asymptotic behavior is reached within about 10% deviation. The results of the next section suggest the following limits for the scaling fields:

Θ-region: $f \lesssim 0.1$

excluded volume region: $f \gtrsim 0.9$

dilute region: $w \gtrsim 0.9$

semidilute region: $w^{1/2} \lesssim 0.1$

In Figure 3a we have plotted these limits as a function of the variables

$$z = \hat{N}^{1/2} = u\frac{T - \Theta}{\Theta}N^{1/2} \tag{3.16}$$

$$x = \hat{c}_1 N^{1/2} = g^*\hat{l}^3 c_1 N^{1/2} \tag{3.17}$$

(Note that in the second part of these equations we have used the two-parameter assumption.)

Within the present model the semidilute Θ-region does not reach the line $z = 0$ ($T \equiv \Theta$) for finite x. This makes an important qualitative difference to the Daoud–Jannink diagram. It is due to our neglect of three-body forces. The existence of three-body forces which do not vanish accidentally at $T \cong \Theta$ leads to an interaction of different chains as soon as they overlap geometrically, even at the Θ-temperature. As a result the semidilute Θ-region reaches the line $T = \Theta$ at some finite value of x. The dimensionless three-body coupling constant $W > 0$ introduces a new

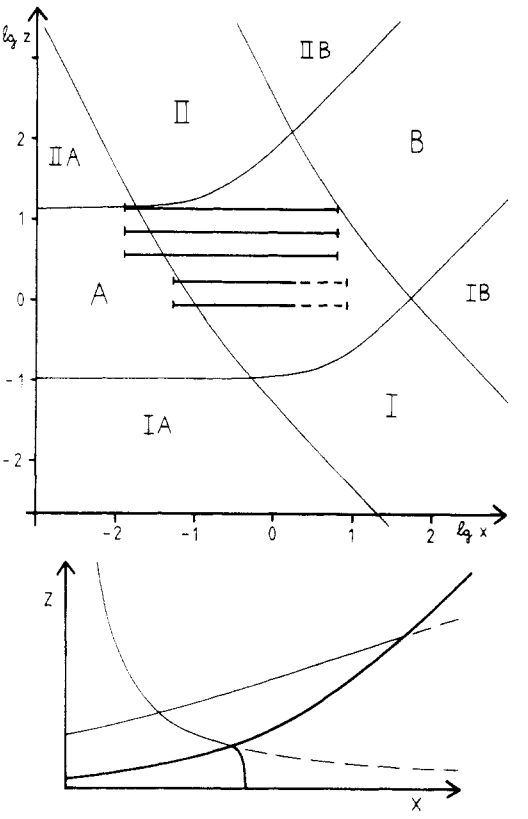

Figure 3. Crossover diagrams in the two-parameter approximation. (a) Boundaries of the limiting regions. A, dilute regime; B, semidilute regime; I, Θ-regime; II, excluded volume regime. The horizontal lines indicate the experimental range of ref 35. (b) Structure of the tricritical Θ-region. Thin lines correspond to $W = 0$ and indicate the crossover dilute ↔ semidilute or Θ-region ↔ excluded volume region. Fat lines indicate the structure of the tricritical domain which is given by[12] $z \lesssim \text{const}\cdot W^{1/2}(W \ln N)^{-3/32} + \text{const}\cdot W(W \ln x^2/N)^{-7/11}x$. At $x \sim (\ln N)^{1/2}$ the tricritical crossover dilute ↔ semidilute takes place.

scale, which makes the diagram more complicated. The tricritical region, where W controls the behavior of the system, has been analyzed in detail by Duplantier.[12] In Figure 3b we have plotted the structure of the Θ-region according to our model, adding crossover lines of the tricritical theory (compare Figure 4 of ref 12). We have chosen a situation in which W is not too big, so that the tricritical region does not cover all of the Θ-region. The tricritical lines depend on the chain length. With increasing N the tricritical region shrinks toward $z = 0$ and the boundary between the dilute and semidilute tricritical regimes tends to $x = \infty$. Thus for very small concentration and extreme values of N, both the tricritical region and the Θ-region could be observed. At present, a general quantitative discussion of the crossover to the tricritical region is missing. This makes a discussion of experiments near $T = \Theta$ somewhat problematic. The analysis presented in the next sections is in favor of a situation as presented in Figure 3b. In the dilute limit $x \to 0$, the tricritical region is too small to be identified whereas for higher concentrations the $W \sim 0$ semidilute Θ-region is not observed.

4. Theoretical Results

4.1. Crossover Functions. In ref 3 we have presented a second-order calculation for the thermodynamic scaling function $\mathcal{P}$ in the excluded volume limit. In first order we now have extended this calculation to the whole critical region. Since the influence of polydispersity on $\mathcal{P}$ is small, we only present results for the exponential ensemble $p(x) = \exp(-x)$ where the calculations are rather simple. (Up to higher order terms this ensemble coincides with des

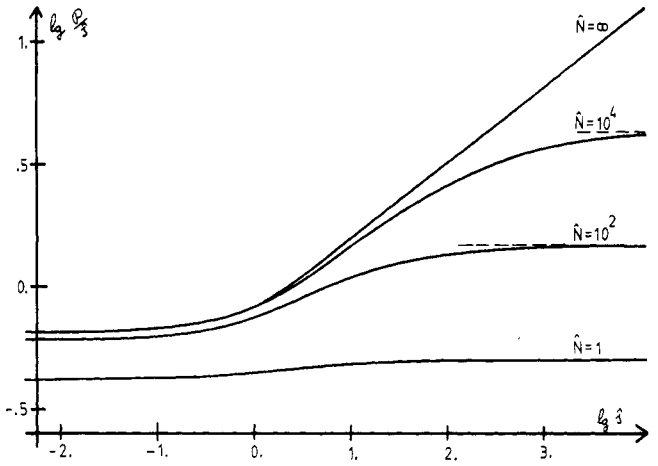

Figure 4. $\log (\mathcal{P}/\hat{s})$ as a function of $\log \hat{s}$ for fixed $\hat{N}$ (i.e., fixed N and T). $\hat{N} = \infty$ represents the excluded volume limit.

Cloizeaux's "equilibrium" ensemble,[19] in which $p(x)$ depends weakly on the overlap.) We find

$$\mathcal{P}(w,f) = \frac{1-w}{4w}\left(1 + \frac{5}{8}\epsilon f\right) + \frac{f}{2}\left[\frac{\epsilon}{8} + \left(\frac{1}{w} - 2\right)G\right] \quad (4.1)$$

where

$$G = \frac{w}{4}\,\frac{w^{-\epsilon/2} - 1}{1-w} \quad (4.2)$$

In the excluded volume limit $f = 1$, this is consistent with our previous result. (Note that the definition of w used here differs from that of ref 3.) In the Θ-region $f << 1$, eq 3.4 and 3.7 can be solved to yield

$$f = \frac{\hat{N}^{\epsilon/2}}{(1 + 2\hat{c}_1\hat{N})^{\epsilon/2}} \quad (4.3)$$

$$w = \frac{1}{1 + 2\hat{c}_1\hat{N}}\left\{1 + \frac{f}{1 + 2\hat{c}_1\hat{N}}\left[\left(2\frac{2 - \nu d}{\nu\omega} + \frac{\epsilon}{2}\right)\hat{c}_1\hat{N} + \frac{1}{2}(1 + 2\hat{c}_1\hat{N})^{\epsilon/2} - \frac{1}{2}\right]\right\} \quad (4.4)$$

$$\mathcal{P} = \frac{1}{2}\hat{c}_1\hat{N} + f\left\{\frac{\epsilon}{16} + \left(\frac{3}{16}\epsilon - \frac{2 - \nu d}{2\nu\omega}\right)\hat{c}_1\hat{N} - \frac{(1 + 2\hat{c}_1\hat{N})^{\epsilon/2} - 1}{16\hat{c}_1\hat{N}}\right\} \quad (4.5)$$

In the semidilute limit $c_1N >> 1$, eq 4.5 reduces to

$$\mathcal{P} = \frac{1}{2}\hat{c}_1\hat{N} + \frac{1}{2}\left(\frac{3}{16}\epsilon - \frac{2 - \nu d}{2\nu\omega}\right)(2\hat{c}_1)^{1-\epsilon/2}\hat{N} \quad (4.6)$$

The structure of the correction term in eq 4.6 was first determined by Edwards.[2] Since we use an ϵ-expansion, the coefficient found here for $d = 3$ differs from that of the simple cluster expansion.

Typically $\mathcal{P}$ is measured as a function of c_1 for fixed T and N, i.e., fixed $\hat{N}$. The overlap

$$\hat{s} = \hat{c}_1\hat{N}^{\nu d-1} = g^*(s_1 s_N{}^{\nu})^d c_p N^{\nu d} \quad (4.7)$$

can be used as a linear measure of c_1. In the excluded volume limit, $\hat{s}$ is the scaling variable replacing the variable s of ref 3: $\hat{s} = 0.425s$. Equations 3.4 and 3.7 yield

$$\hat{s} = \tfrac{1}{2}(1-w)w^{1-\nu d}[1 + \epsilon/8 + G]^{\nu d}; \qquad (f = 1) \quad (4.8)$$

In Figure 4 we have plotted $\ln (\mathcal{P}/\hat{s})$ as a function of $\ln \hat{s}$ for several values of $\hat{N}$. For large $\hat{N}$ the double crossover discussed in the previous section is clearly exhibited. It may be difficult to observe experimentally the second crossover leading to the semidilute Θ-regime. This needs extremely long chains since otherwise this limit is dominated by the semidilute tricritical region. Furthermore, we have found[20] that experiments typically cover a range $\hat{s} \lesssim 20$ and therefore do not reach the second crossover region.

We next consider the zero-momentum limit of the density correlation function $I_c(q)$. We write

$$I_c(0) = c_p N^2 J_c(0) \quad (4.9)$$

For a monodisperse system $J_c(0)$ can be expressed in terms of the osmotic compressibility

$$J_c^{-1}(0) = 1 + \left(1 + \hat{s}\frac{\partial}{\partial \hat{s}}\bigg|_{\hat{N}=\text{const}}\right)\mathcal{P}(w,f) \quad (4.10)$$

For general polydispersity $J_c(0)$ and $\mathcal{P}$ are independent observables. The expression for $J_c(0)$ is complicated. For a monodisperse system we find

$$J_c(0) = w\left(1 + \frac{2wK^{(2,0)}}{1-w}\right)\left\{(1 + K^{(2,0)})\left[w + \frac{\epsilon}{2}fw^2\left(\frac{\ln w}{2(1-w)}\left(\frac{2+w}{1-w} - \frac{3}{2}\right) + \frac{3}{2(1-w)} + \Delta_1\right)\right] + \frac{1-w}{2}\left(1 + \frac{\epsilon}{2}f\right)[1 + f(\epsilon/8 + G)]^2\right\}^{-1} \quad (4.11)$$

where

$$K^{(2,0)} = f/8(1 - w^{-\epsilon/2}) - \frac{\epsilon}{16}f \ln \frac{1+w}{2} \quad (4.12)$$

and G is given in eq 4.2. The correction term Δ_1 can be evaluated only numerically. Within at most 1% deviation in $J_c(0)$ the result can be parametrized as

$$\Delta_1 = -\frac{1}{8} - 0.02(1-w) - 0.24(1 - w^{1/2})^4\frac{1 + 0.66w^{1/2} - 3w}{1 - 0.7w^{1/2}} + \frac{\ln (1+w)/2}{1-w} \quad (4.13)$$

Equations 4.11 to 4.13 will be used in the analysis of experiments. In the excluded volume limit the result deviates less than 1% from the result based on the second-order calculation[3] of $\mathcal{P}$. To show the influence of polydispersity, in Figure 8 we have plotted $J_c(0)$ for both the monodisperse and the exponential ensembles in the excluded volume limit. A large part of the polydispersity correction is taken into account by the form

$$J_c^{-1}(0, p(x)) = \frac{1}{\tilde{p}''} - 1 + J_{c,\text{mono}}{}^{-1}(0) \quad (4.14)$$

suggested by the mean field expression.

In the semidilute limit $J_c(0)$ is expected to be independent of polydispersity. This is supported by our calculation, which yields

$$J_c(0) = \frac{2w(1 + \mathcal{O}(w^{1/2}))}{(1 + \epsilon f/2)(1 + \epsilon f/8)^2} \quad (4.15)$$

for all $p(x)$. The strongest polydispersity effects are found in the dilute limit. Defining the second virial coefficient for light scattering $A_2{}^{ls}$ by

$$J_c(0)^{-1} = \tilde{p}''^{-1} + 4A_2{}^{ls}\frac{\hat{c}_1}{\hat{N}} + \mathcal{O}(\hat{c}_1{}^2) \quad (4.16)$$

we find

$$A_2^{ls} = \tfrac{1}{4} f^{4/\epsilon}(1-f)^{-d/\omega}\bar{A}_2 \tag{4.17}$$

where

$$\bar{A}_2 = 1 + \frac{77}{96}\epsilon f, \qquad \text{exponential ensemble} \tag{4.18a}$$

or

$$\bar{A}_2 = 1 + 1.069\epsilon f, \qquad \text{monodisperse} \tag{4.18b}$$

We note that for $f \to 1$ the first-order corrections become very large. For $\epsilon = 1$ the results (4.17) and (4.18) are plotted in Figure 5 as a function of $z = \hat{N}^{\epsilon/2}$.

The radius of gyration depends strongly on polydispersity. Most of this dependence is cancelled if we consider the swelling factor

$$\alpha_g^2 = R_g^2/R_0^2 \tag{4.19}$$

where

$$R_0^2 = -\frac{\tilde{p}'''}{3\tilde{p}''} ds_1^2 \hat{N} \tag{4.20}$$

reduces to the radius at the Θ-point, $R_\Theta^2 = -(\tilde{p}'''/\tilde{p}'')(d/3)\hat{l}^2 N$, provided the two-parameter assumption (3.13) and (3.14) holds. We note that α_g^2 as defined here is a universal function of $z = \hat{N}^{\epsilon/2}$. It may differ from the experimentally observed swelling factor since in general $R_0^2 \neq R_\Theta^2$. This well-known fact recently has been stressed in ref 6. Our calculation yields

$$\alpha_g^2 = \frac{(1-f)^{(1/\nu-2)/\omega}}{1 + f(\epsilon/8 + G)}[1 + \epsilon f \Delta_2] \tag{4.21}$$

Here, $\Delta_2 = \Delta_2(w)$ in general can be calculated only numerically. For the monodisperse ensemble and $d = 3$ the result can be parametrized as

$$\Delta_2 = 0.062 - 0.240w^{1/2} - 0.008w + 0.265w^{3/2} - 0.142w^2 \tag{4.22}$$

In the discussion relating to eq 2.30 we also need the exact form of Δ_2 in the large-overlap region:

$$\Delta_2 = \frac{1}{16} - \frac{1}{\epsilon}G + O(w) \tag{4.22a}$$

In the semidilute limit α_g^2 does not depend on polydispersity.

$$\alpha_g^2 = (1-f)^{(1/\nu-2)/\omega}\frac{1 + (\epsilon/16)f}{1 + (\epsilon/8)f}; \qquad (w = 0) \tag{4.23}$$

The strongest effect of polydispersity is again found in the dilute limit. The full result reads

$$\alpha_g^2 = \frac{(1-f)^{(1/\nu-2)/\omega}}{1 + f\epsilon/4}[1 + \epsilon f \Delta(\tilde{p})]; \qquad (w = 1) \tag{4.24}$$

$$\Delta(\tilde{p}) = -\frac{39}{288} + \frac{3}{4\tilde{p}'''}\int_0^\infty \frac{dy}{1+y}(\tilde{p}''(y) - \tilde{p}(y)) + \frac{1}{8\tilde{p}'''}\int_0^\infty dy\, \tilde{p}''''(y) \ln y \tag{4.25}$$

In the monodisperse limit this reduces to $\Delta = -0.063$; for the exponential ensemble we find $\Delta = {}^3/_{32}$. For both ensembles the result (4.24) is plotted in Figure 6. In the excluded volume limit the swelling factor is not a useful quantity since it masks the fact that this limit involves only the single scale

$$B = s_1 s_N^{\nu} \tag{4.26}$$

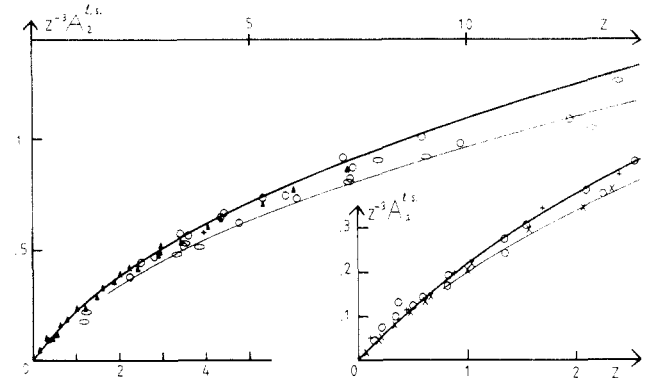

Figure 5. $z^{-3}A_2^{ls}$ as a function of z. The fat or thin lines give the results for the monodisperse or the exponential chain length distribution, respectively. Data: (▲) poly(isobutylene)–isoamyl isovalerate;[29] (×) poly(α-methylstyrol)–cyclohexane;[30] (○) polystyrene–*trans*-decalin;[28] (+) polystyrene–cyclohexane;[27] (○) poly(chloroprene)–*trans*-decalin.[25]

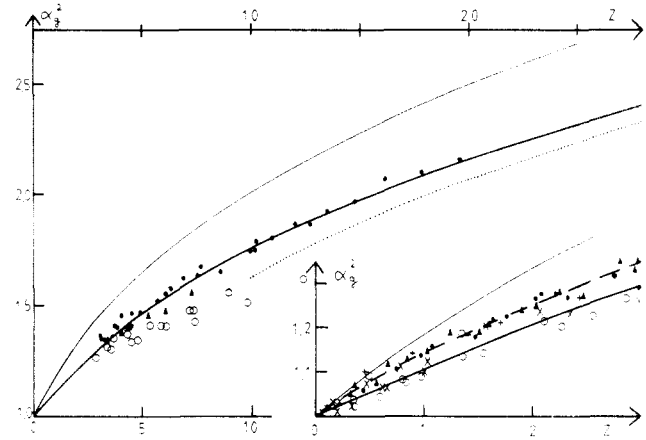

Figure 6. α_g^2 as a function of z. The fat or thin lines give the results for the monodisperse or the exponential chain length distribution, respectively. The dotted line gives the asymptotic behavior for the monodisperse ensemble. The broken line in the insert gives the semiempirical result of Domb and Barrett.[44] Data: (●) polystyrene–cyclohexane;[24] other symbols as in Figure 5.

This scale occurs in the definition of the overlap variable (4.7), $\hat{s} = g^* B^d c_p N^{\nu d}$ and it determines the length scale of R_g. We find

$$R_g^2 = B^2\left(-\frac{d}{3}\frac{\tilde{p}'''}{\tilde{p}''}\right)N^{2\nu}w^{-1}\left(\frac{w}{1 + \epsilon/8 + G}\right)^{2\nu}[1 + \epsilon\Delta_2]; \qquad (f = 1) \tag{4.27}$$

This result is plotted in Figure 10 as a function of $\hat{s}$ (eq 4.8).

Our discussion can be repeated for the density correlation length ξ^2. Polydispersity effects are strong and influence nontrivially even the mean field order. Defining

$$\alpha_\xi^2 = \xi^2/R_0^2 \tag{4.28}$$

we find

$$\alpha_\xi^2 = \frac{w}{w + (1-w)\tilde{p}''/2}(1-f)^{(1/\nu-2)/\omega}; \qquad \text{(mean field)} \tag{4.29}$$

For the monodisperse ensemble we have the first-order result

$$\alpha_\xi^2 = \frac{(1-f)^{(1/\nu-2)/\omega}}{1 + f(\epsilon/8 + G)}\frac{2w}{1+w}[1 + \epsilon f \Delta_3]^{-1} \tag{4.30}$$

with the parametrization

$$\Delta_3 = 0.126 + 0.492(1 - w) + \frac{3(1 - w^{1/2})^3}{5 + 4w^{1/2}}; \qquad (\epsilon = 1) \tag{4.31}$$

In the dilute limit α_ξ^2 coincides with α_g^2. In the semidilute limit ξ^2 still shows some nontrivial polydispersity dependence, in contrast to simple expectations.

$$\xi^2 = -\frac{2}{3}d\frac{\tilde{p}'''}{(\tilde{p}'')^2}s_1^2 f^{2/\epsilon}(1 - f)^{-2/\omega} \times \left[1 + \epsilon f\left(\frac{7}{16} - \frac{25}{32}\frac{(\tilde{p}'')^2}{\tilde{p}'''}\right)\right]^{-1}; \qquad (w = 0) \tag{4.32}$$

In the excluded volume limit the result analogous to eq 4.27 is (monodisperse ensemble)

$$\xi^2 = B^2\frac{d}{3}N^{2\nu}\left(\frac{w}{1 + \epsilon/8 + G}\right)^{2\nu}\frac{2}{1 + w}[1 + \epsilon\Delta_3]^{-1}; \qquad (f = 1) \tag{4.33}$$

This is plotted in Figure 9 together with the corresponding result in the exponential ensemble.

In section 2 we identified Edward's screening length with the density correlation length ξ. A more detailed analysis suggests another definition in terms of the "size of the correlation hole" ξ_h,[2,16] which is related to but not identical with ξ. This length scale can be defined properly only in the semidilute limit, where ξ is determined as

$$\xi^2 = -\mathrm{d}\lim_{w\to 0}\left.\frac{\partial}{\partial q^2}\right|_0 \ln J_c(q) \tag{4.34}$$

Interchanging the limits, we find ξ_h.

$$\xi_h^2 = -\mathrm{d}\left.\frac{\partial}{\partial q^2}\right|_0 \lim_{w\to 0} \ln (J_c(q)/w) \tag{4.35}$$

Our calculation yields

$$\xi_h^2 = ds_1^2 f^{2/\epsilon}(1 - f)^{-2/\omega}\left[1 + \frac{23}{24}\epsilon f\right]^{-1} \tag{4.36}$$

independent of polydispersity. It turns out that ξ_h coincides with the density correlation length of the equilibrium ensemble. An inspection of our results for the momentum dependence of $J_c(q)$ yields the following explanation of the role of ξ or ξ_h: ξ determines the q dependence of $J_c(q)$ in the range $q < R_g^{-1}$, where $J_c(q)$ depends on polydispersity. For $q >> R_g^{-1}$ the polydispersity dependence vanishes, and since $R_g^{-1} \to 0$ in the semidilute limit, we are able to define *in that limit* a correlation length independent of $p(x)$. This length ξ_h governs the momentum dependence in the range $\xi_h^{-1} >> q > R_g^{-1} \to 0$. Light scattering experiments typically measure ξ. ξ_h has been determined approximately by neutron scattering. In the excluded volume limit $f \to 1$ or the Θ-limit $f \to 0$ both correlation lengths scale in the same way but their crossover behavior is different.

4.2. Critical Ratios. As mentioned above, the polymer system in the excluded volume limit possesses only a single nonuniversal scale B. We can eliminate this scale in favor of some observable quantity using, for instance, eq 4.27 in the dilute limit. In this way we construct fully universal scaling functions depending on $\tilde{s} = c_p R_g^d$. (Besides leading to complete universality, the variable $\tilde{s}$ has the additional virtue of reducing to the appropriate scaling variables in both the excluded volume limit, $\tilde{s} \sim c_p N^{\nu d}$, and the Θ-limit, $\tilde{s} \sim c_p N^{d/2}$. In our calculations we nevertheless prefer $\hat{s}$ because use of $\tilde{s}$ mixes the theoretical (or experimental) uncertainties of R_g^2 with those of the scaling function considered.) In the limits $\tilde{s} \to 0$ or $\tilde{s} \to \infty$ some of the fully universal scaling functions tend to finite values known as "critical ratios". More generally, a critical ratio[21,22] is a combination of limiting values of observables constructed such that B cancels. A simple example is given by the ratio ξ_h^2/ξ^2 in the semidilute excluded volume limit.

From a theorist's point of view, critical ratios have the attractive feature that they allow for a straightforward ϵ-expansion which is independent of the special realization of the RG. They therefore do not suffer from the ambiguities inherent in a low-order calculation of crossover functions. (This statement needs certain qualifications given below.) From an experimentalist's point of view, critical ratios may be less useful. The limiting values of interest usually cannot be extracted unambiguously from experiment without use of theoretical information on the $\hat{s}$ dependence of the scaling functions. On a practical level we therefore are back to fitting the full functions.

In the following we consider some of the more important critical ratios. One prominent example[22] is the excluded volume limit of the interpenetration function

$$\psi = \frac{1}{8\pi^{3/2}}\frac{N_w^2}{R_g^3}\left.\frac{\partial}{\partial c_1}\right|_0\left(\frac{c_1}{I_c(0)}\right) = \frac{g^*}{2\pi^{3/2}}s_1^3\frac{A_2^{ls}}{R_g^3}(\tilde{p}'')^2 \tag{4.37}$$

Equations 4.17 to 4.20 and eq 4.24 yield for a monodisperse system

$$\psi = \frac{g^*}{8\pi^{3/2}}f\frac{1 + 1.069\epsilon f}{(1 - 0.063\epsilon f)^{2-\epsilon/2}} \tag{4.38}$$

In our approach the fixed-point coupling takes the value

$$g^* = (4\pi)^{d/2}\Gamma(d/2)\left[\epsilon/8\left(1 + \frac{5}{32}\epsilon + \mathcal{O}(\epsilon^2)\right)\right] \tag{4.39}$$

where $\Gamma()$ denotes the gamma function. With this expression the ϵ-expansion of $\psi^* = \psi(f = 1)$ reads

$$\psi^* = (4\pi)^{(d-3)/2}\Gamma(d/2)[\epsilon/8(1 + 1.351\epsilon + \mathcal{O}(\epsilon^2))] \tag{4.40}$$

According to the usual conventions the prefactor $(4\pi)^{(d-3)/2}\Gamma(d/2)$ is not expanded. For $\epsilon = 1$ the value $\psi^* = 0.260$ results. Now it is clear that we have some freedom in treating g^*. For instance, we could have chosen to expand also the prefactor. Furthermore, the definition of g^* is not unique and different choices may involve different not expanded factors. Thus low-order estimates for critical ratios involving g^* are somewhat arbitrary.[5,6,22,42] The occurrence of explicit factors of g^* can always be traced back to the factor of g^* relating the concentration scale g^*B^d to the length scale B. It is the relation between these two scales that is not fixed uniquely in a low-order calculation.

These observations suggest giving up the idea of a strict ϵ-expansion for the critical ratios. In agreement with our general attitude (see also ref 6), we rather expand the scaling functions only, thus evaluating ψ^* from eq 4.38 instead of eq 4.40. We use g^* as a theoretical parameter *adjusted such that ψ^* takes the value $\psi^* \cong 0.245$ observed experimentally.*[23] The resulting value $g^* = 4.8$ is not too different from the value $g^* = 5.7$ given by eq 4.39.

Within this scheme we have calculated some critical ratios relating the $\hat{s} \to 0$ and $\hat{s} \to \infty$ limits of scaling functions.

$$\mathcal{R}_g = \lim_{\hat{s}\to 0}\left(-\frac{\tilde{p}''}{\tilde{p}'''}R_g^2\right) \times \lim_{\hat{s}\to\infty}\left[c_p^{(2\nu-1)/(\nu d-1)}\left(-\frac{\tilde{p}''}{\tilde{p}'''}R_g^2\right)\right]^{-2(\nu d-1)/(d-2)} \tag{4.41}$$

$$\mathcal{R}_\xi = \lim_{\hat{s}\to 0}\left(-\frac{\tilde{p}''}{\tilde{p}'''}\xi^2\right)\lim_{\hat{s}\to\infty}\left[c_p{}^{2\nu}\left(-\frac{(\tilde{p}'')^2}{\tilde{p}'''}\xi^2\right)^{\nu d-1}\right] \quad (4.42)$$

$$\mathcal{R}_h = \lim_{\hat{s}\to 0}(R_g{}^2)\lim_{\hat{s}\to\infty}[c_p{}^{2\nu}\xi_h{}^{2(\nu d-1)}], \qquad \text{monodisperse} \quad (4.43)$$

These ratios characterize the overall shape of the corresponding scaling functions. (A ratio for $\mathcal{P}$ has been calculated in ref 20.) Another useful ratio determines the behavior of ξ^2 at small overlap:

$$\xi^2 = \xi^2(\hat{s}=0)[1 - A_\xi c_p\xi^d(\hat{s}=0) + \mathcal{O}(c_p\xi^d)^2] \quad (4.44)$$

$$A_\xi = -\lim_{\hat{s}\to 0}\left(\xi^{-2-d}\frac{\partial}{\partial c_p}\xi^2\right) \quad (4.45)$$

For ξ_h we also can define a universal quantity

$$r_h = B^{2/(\nu d-1)}c_1{}^{2\nu/(\nu d-1)}\xi_h{}^2 \quad (4.46)$$

which does not need information on N or $p(x)$. This will be useful for a comparison to experiment.

Finally we calculate

$$\Psi_\infty{}^* = \xi_h{}^d\lim_{\hat{s}\to\infty}\frac{\Pi}{k_BT} = \xi_h{}^d\lim_{\hat{s}\to\infty}[c_p\mathcal{P}(\hat{s})] \quad (4.47)$$

where Π denotes the osmotic pressure. This ratio is the semidilute counterpart of the interpenetration ratio ψ^*. The values of all these ratios are given in Table I for both the monodisperse and the exponential ensemble. To show the effect of the first-order corrections we have given also results in which the mean field expressions have been used for the scaling functions. In most cases the first-order correction is quite large, and therefore our estimates give the order of magnitude rather than a precise value. It, however, is interesting to note that the convergence generally is improved if we use ψ^* to eliminate explicit powers of g^* due to the relation between concentration scale and length scale. This is demonstrated by the results for A_ξ/ψ^* or $\mathcal{R}_\xi\psi^{*2\nu}$ in Table I. Only in $\mathcal{R}_g$ does this procedure increase the first-order correction ($\mathcal{R}_g \to \mathcal{R}_g\psi^{*2(1-2\nu)}$).

Critical ratios can be calculated also outside the excluded volume limit. The discussion becomes especially simple if the two-parameter assumption holds. In that case $R_g{}^2$ (eq 4.20) and thus $\alpha_g{}^2$ (eq 4.19) are directly observable. We can use $\alpha_g{}^2(z)$ to eliminate $z = \hat{N}^{\epsilon/2}$ from other scaling functions, thus constructing fully universal scaling functions depending on $\tilde{s} = c_pR_g{}^d$ and $\alpha_g{}^2$. We then can consider for instance critical ratios connecting the Θ-limit to the excluded volume limit. We do not pursue this subject further here.

5. Comparison to Experiment

5.1. Temperature Crossover in the Dilute Limit. The dilute limit has often been the subject of detailed investigations.[1,4-6] It is not our purpose here to compare the different calculations; rather we compare our results to experimental data. In our analysis we use the two-parameter assumption, which is justified exprimentally for all systems we consider.

Figures 5 and 6 contain results for $z^{-3}A_2{}^{ls}$ and $\alpha_g{}^2$, respectively. The parameter values used for z (eq 3.16) and $\hat{l}$ are collected in Table II. We should stress that parameters like $\hat{l}$, u, and B are effective quantities defined in the univeral regime of very long chains. Theoretically there is no simple connection to chemical parameters specifying a single monomer. Still there might exist an empirical relation which could be exhibited by studying a large number of chemically different systems. Figure 5 shows that the data for $A_2{}^{ls}$ are adequately represented by our theory. There is no systematic deviation and the precision of the data is not high enough to show the polydispersity effects. For $\alpha_g{}^2$ the situation is more complicated. The data given as filled symbols recently have been used by Miyaki and Fujita[24] to extract the universal scaling function. These data show few intrinsic scatter and are assumed to be very precise. They closely follow the empirical law given by Domb and Barrett.[44] For $z \lesssim 10$ our calculation underestimates $\alpha_g{}^2$ with respect to these data, which cannot be explained as a polydispersity effect. It rather gives an indication of the error involved in our calculation. In Figure 6 we have included some data[25] (open circles) that show the problems encountered in extracting the scaling function. (The often-used data of ref 26 are intermediate between these data and the universal curve.) We believe that such large deviations from universality are due to systematic errors in extrapolating the observed data to $q = 0$, $c_1 = 0$. The deviations found for $\alpha_g{}^2$ are the source of corresponding deviations in ψ, which as function of $\alpha_g{}^2$ is given in Figure 7. For small $\alpha_g{}^2$ our calculation has a tendency to overestimate ψ. Again the accuracy of the data is not high enough to show the influence of polydispersity, even though the theory predicts a large effect.

5.2. Concentration Crossover in the Excluded Volume Limit. Figures 8–10 show a comparison of results of our calculation to experimental data on the small-momentum behavior in the excluded volume limit. Obviously, the agreement between theory and experiment is very

Table I

	monodisperse		exponential	
	mean field	first order	mean field	first order
ψ^*	0.108	0.246	0.084	0.132
$\mathcal{R}_g$	2.22	1.67	2.22	2.01
$\mathcal{R}_\xi$	0.119	0.053	0.119	0.071
$\mathcal{R}_h$	0.162	0.080		
A_ξ	6.5	12.4	2.2	3.5
r_h	0.103	0.056	independent of $p(x)$	
$\psi^*{}_\infty$	0.136	0.081	independent of $p(x)$	
A_ξ/ψ^*	60	50	26.2	26.5
$\mathcal{R}_\xi\psi^{*2\nu}$	0.87×10^{-2}	1.02×10^{-2}	0.65×10^{-2}	0.66×10^{-2}

Table II
Parameter Values within the Two-Parameter Regime

system	l, 10^{-8} cm	Θ, K	u
polystyrene–cyclohexane[24,27]	2.94	307.7	0.57
polystyrene–*trans*-decalin[28]	2.82	292.7	0.57
poly(isobutylene)–isoamyl isovalerate[29]	2.25	295.3	0.21
poly(α-methylstyrene)–cyclohexane[30]	3.26	308.2	0.4
poly(chloroprene)–*trans*-decalin[25]	2.60	275.1	0.58

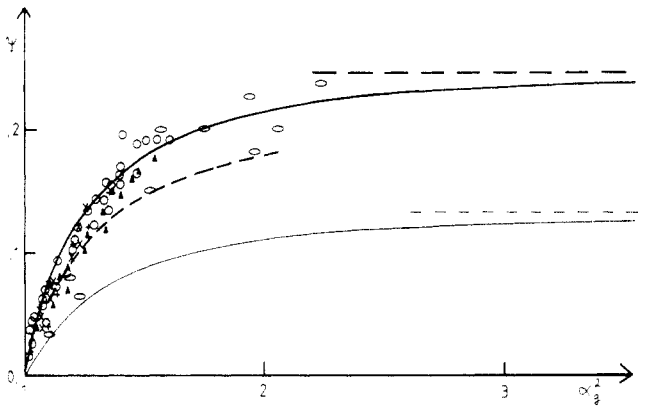

Figure 7. Interpenetration ratio ψ as a function of $\alpha_g{}^2$. The fat or thin lines give the results for the monodisperse or the exponential ensemble, respectively. Broken horizontal lines represent the values ψ^* in the excluded volume limit. The broken curve corresponds to a Schulz distribution with $M_w/M_n = 1.1$. Symbols for data as in Figure 5.

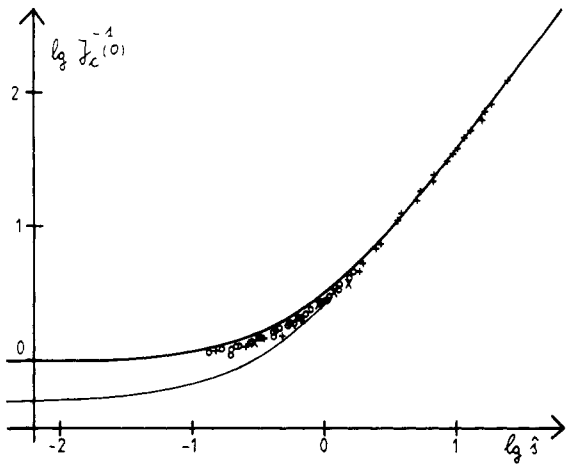

Figure 8. $\log J_c^{-1}(0)$ as a function of $\log \hat{s}$ in the excluded volume limit. The fat or thin lines give the results for the monodisperse or the exponential ensemble, respectively. Data: (×) PS–benzene;[28] (○) PS–benzene;[31] (+) poly(α-methylstyrene)–toluene.[32]

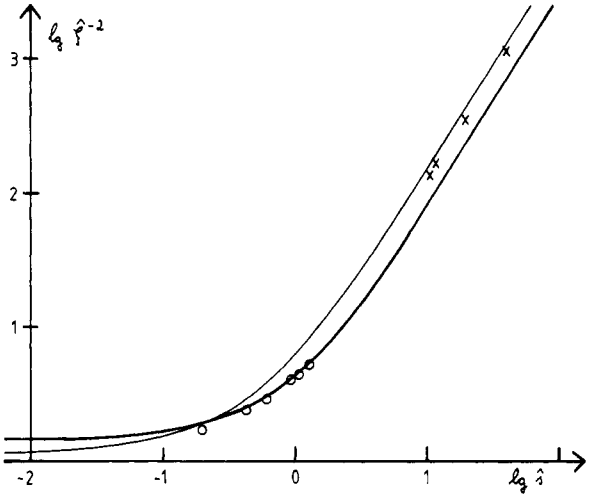

Figure 9. $\log \hat{\xi}^{-2}$ as a function of $\log \hat{s}$. $\hat{\xi}$ is defined as $\hat{\xi}^2 = N^{-2\nu}B^{-2}(-\bar{p}''/\bar{p}''')\xi^2$, which in the monodisperse ensemble reduces to $\hat{\xi}^2(\hat{s}) = 0.68\xi^2(\hat{s})/\xi^2(0)$. The fat or thin lines give the results for the monodisperse or the exponential ensemble, respectively. Data: (○) PS–benzene.[31] Crosses give results[33] for $^1/_3B^{-2}N^{-2\nu}\xi_h^2$.

Table III
Parameter Values in the Excluded Volume Limit

system	B, 10^{-8} cm
polystyrene–benzene[31]	2.40
polystyrene–CS_2[33]	2.62
poly(α-methylstyrene)–toluene[32]	2.25

good. We recall that in the excluded volume limit each chemical system depends on a single nonuniversal scale B. The values of this parameter used here are collected in Table III. They all correspond to temperatures around $T \sim 25$ °C. For the polystyrene (PS)–benzene system, B has been determined from the R_g^2 data in the dilute limit analyzed in ref 31. For the other systems, B is deduced from the fits given here. For the system poly(α-methylstyrene)–toluene this value is slightly lower than the value $B \sim (2.31\text{–}2.37) \times 10^{-8}$ cm extracted[20] from osmotic pressure data of the same authors. This cannot be an artifact of the theory since our result for $J_c(0)$ in the monodisperse ensemble coincides with that calculated from $\mathcal{P}(s)$ (ref 20, eq 2.2) via the compressibility relation (4.10).

Because of the relation of $J_c(0)$ to $\mathcal{P}(s)$, the fit of Figure 8 just supports our previous conclusions[20] based on osmotic pressure data. Independent evidence on the quality of the theory is provided by the determination of ξ^2 and R_g^2.

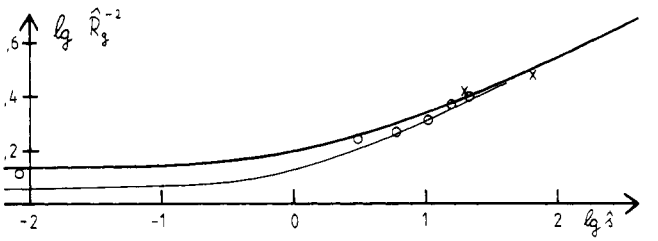

Figure 10. $\log \hat{R}_g^{-2}$ as a function of $\log \hat{s}$. $\hat{R}_g$ is defined as $\hat{R}_g^2 = N^{-2\nu}B^{-2}(-\bar{p}''/\bar{p}''')R_g^2$, which in the monodisperse ensemble reduces to $\hat{R}_g^2(\hat{s}) = 0.72R_g^2(\hat{s})/R_g^2(0)$. (The difference of the coefficient 0.72 compared to 0.68 for $\hat{\xi}^2$ is an $\mathcal{O}(\epsilon^2)$ effect.) The fat or thin lines give the results for the monodisperse or the exponential ensemble, respectively. Data for PS–CS_2:[33] (○) $M_w = 1.14 \times 10^5$; (×) $M_w = 5 \times 10^5$.

Published data on ξ^2 are rare; those given in Figure 9 are obtained from Figure 2 of ref 31. In this figure we also have included some neutron scattering data on ξ_h^2. According to section 4, these data should fall close to the results for ξ^2 in the exponential ensemble, and this is indeed the case. The best way to analyze ξ_h^2 may be to extract the ratio r_h defined in eq 4.46. The data on PS–CS_2 given in ref 33 yield values $0.072 \lesssim r_h \lesssim 0.081$ with an average $\bar{r}_h = 0.078$. In ref 34 data on PS–benzene are given which scatter strongly, however. In the range $10 \lesssim \hat{s} \lesssim 200$ values $0.043 \lesssim r_h \lesssim 0.12$, $\bar{r}_h \cong 0.071$ are found. In view of the large uncertainty of both the theoretical and the experimental estimates we feel that the agreement with the value $r_h \cong 0.056$ give in Table I is satisfactory. From the R_g^2 data we also can extract the relevant ratio $\mathcal{R}_g$. We find values $1.80 \lesssim \mathcal{R}_g \lesssim 2.16$ with an average $\bar{\mathcal{R}}_g \cong 1.85$. This is in good agreement with the theoretical value given in Table I, and the agreement is improved by noting that the polydispersity of the sample ($M_w/N_n \cong 1.1$) increases the theoretical estimate from the monodisperse value to about 1.74.

5.3. Combined Temperature and Concentration Crossover. A systematic study covering a large part of the crossover diagram for the system PS–*trans*-decalin has recently been published by Nose and Chu.[35] Temperature and concentration dependences of $J_c(0)$ and ξ^2 were measured for two samples of chain lengths $N \cong 1.7 \times 10^3$ or $N \cong 1.1 \times 10^5$. For fixed T the range of $x = g^*\hat{l}^3c_1N^{1/2}$ covered by these experiments is represented by the horizontal lines in Figure 3a. We use the parameter values of Table I which also have been used in our analysis of independent data in the dilute limit. For the shorter system $J_c(0)$ near $T = \Theta$ becomes strongly dependent on c_1 for values $c_1 \gtrsim c_1^0 = 4 \times 10^{-4}$ mol cm^{-3}. This sets an upper bound to the range of validity of our theory which neglects all tricritical effects due to three-body interactions. The broken lines in Figure 3a correspond to the region $c_1 > c_1^0$. Figure 11 represents our fit of the data for $J_c(0)$. The calculated curves are corrected for polydispersity effects according to eq 4.14. Serious deviations exist only for $c_1 > c_1^0$, a region that is tested only for the shorter system. For the longer system there are indications of a small systematic error for large overlap, too. As expected from Figure 3a, none of these experiments reaches the semidilute excluded volume limit where $\xi^2 \sim c_1^{1/(\nu d-1)}$. In Figure 12, a subset of the same data is plotted as a function of T.

Figure 13 compares theoretical and experimental results on ξ^2 for the longer chains. (For the shorter chains only a few data on ξ^2 are published.) The agreement is very good, except for the region of *small* c_1. This is surprising since we have found in section 5.1 that our calculation adequately describes the dilute limit. Indeed, the results

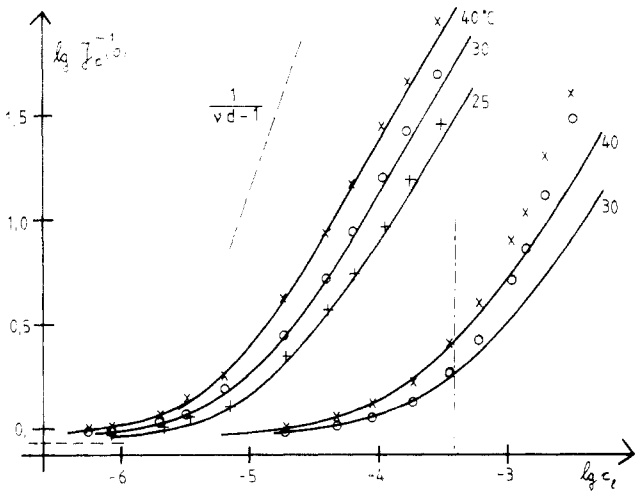

Figure 11. $\log J_c^{-1}(0)$ as a function of $\log c_l$, where c_l is measured in mol cm^{-3}. The three upper curves correspond to the longer chains. The broken vertical line indicates $c_l^0 = 4 \times 10^{-4}$ mol cm^{-3}. Experimental points are taken from ref 35.

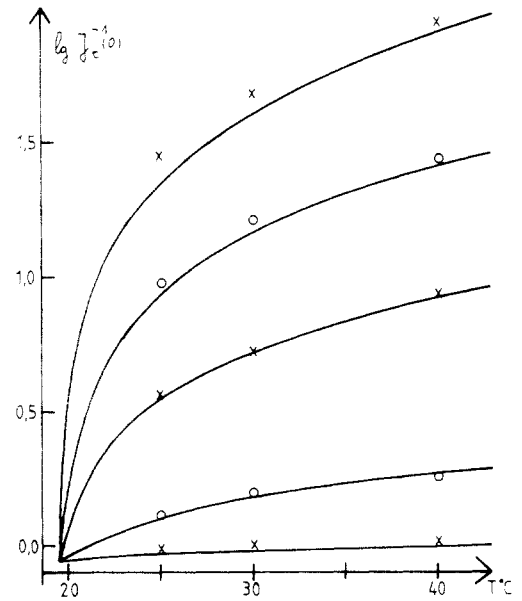

Figure 12. $\log J_c^{-1}(0)$ as a function of T for different concentrations. We have plotted only a subset of the data of ref 35 for the sample of longer chains.

for α_g^2 in the dilute limit given in Table I of the second paper of ref 35 deviate strongly from the universal scaling function of Figure 6 and are not consistent with the results of Fukuda et al.[28] As we have mentioned before, the accurate determination of $\alpha_g^2(c_l \to 0)$ seems to be difficult. For $T \cong \Theta$ the experiment finds pronounced structure in the data for the longer chains, which is traced back to the proximity of the collapsing transition at $T < \Theta$. Such effects are clearly beyond the range of the present theory. With these necessary qualifications we can state that our theory gives a remarkably good fit in the total crossover region. We want to stress again that the fit involves only two parameters, one of which ($\hat{l}$) is determined independently by measuring R_g^2 at $T = \Theta$.

5.4. Temperature Crossover in the Semidilute Limit. For the system PS–cyclohexane the lengths R_g and ξ_h in the semidilute limit have been determined[18] by neutron scattering. We have shown in section 5.1 that our calculation adequately represents the dilute limit for this system. Furthermore, there exist old osmotic pressure data[36] covering a region in the center of the crossover diagram 3a, which—within their limited accuracy—also

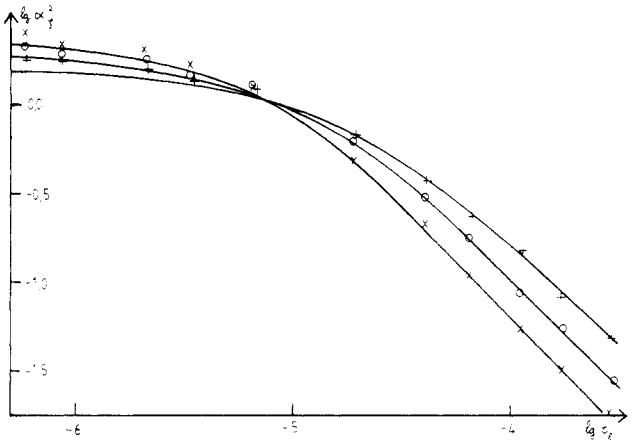

Figure 13. $\log \alpha_\xi^2$ as a function of $\log c_l$. The curves correspond to fixed temperature: $T = 25$, 30, 40 °C from bottom to top at small c_l. To determine $\alpha_\xi^2 = \xi^2/R_0^2$ the data of ref 35 have been reduced with a value $R_0^2 = 1.11 \times 10^6$ Å^2 following from ref 28.

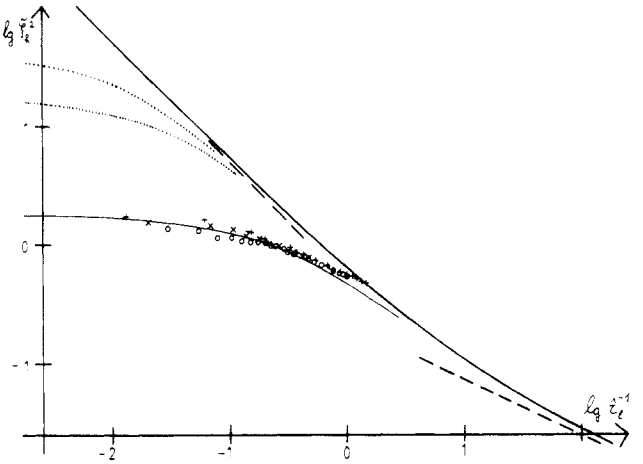

Figure 14. $\log \tilde{\xi}_h^2$ as a function of $\log \hat{c}_l^{-1}$. The fat curve represents the semidilute limit. Broken lines give the asymptotic behavior. Dotted lines are calculated from the density correlation length of the equilibrium ensemble. The parameter values for the experimentally used[18] system with $c_l = 0.058$ g cm^{-3} (lower curve) or $c_l = 0.082$ g cm^{-3} (upper curve) have been used. The thin line represents eq 5.3. Data for PS–cyclohexane:[18] (+) $c_l = 0.058$; (×) $c_l = 0.082$; (○) $c_l = 0.179$ g cm^{-3}.

confirm our theory. In the semidilute limit the situation turns out to be more complicated.

In Figure 14 we have plotted

$$\tilde{\xi}_h^2 = \tfrac{1}{3}\hat{l}^4 g^{*2} c_l^2 \xi_h^2 \tag{5.1}$$

as a function of $\hat{c}_l^{-1}$, where according to eq 3.8, 3.11, 3.13, and 3.14

$$\hat{c}_l^{-1} = \frac{u}{g^*}\frac{T-\Theta}{\Theta}(\hat{l}^3 c_l)^{-1} \tag{5.2}$$

holds in the two-parameter regime. $\tilde{\xi}_h^2$ is a universal quantity depending only on $\hat{c}_l$ ($w = 0$). Figure 14 clearly shows the temperature crossover from a behavior $\tilde{\xi}_h^2 \sim \hat{c}_l^{(4\nu-2)/(3\nu-1)}$ in the excluded volume limit to $\tilde{\xi}_h^2 \sim \hat{c}_l$ in the Θ-limit. $\tilde{\xi}_h^2$ diverges as $T \to \Theta$. We have pointed out in section 3 that the vanishing of f_0 as $T \to \Theta$ produces a second crossover from the semidilute to the dilute Θ-regime (curve 3 in Figure 2). This second crossover depends on $\hat{N}$ (or z, equivalently) in addition to $\hat{c}_l$. To include it we have identified $\tilde{\xi}_h$ with the density correlation length ξ of the equilibrium ensemble and have calculated the latter for the experimental parameter values. As shown by the dotted lines in Figure 14 this second crossover cuts off the divergence. In Figure 14 we have included the experi-

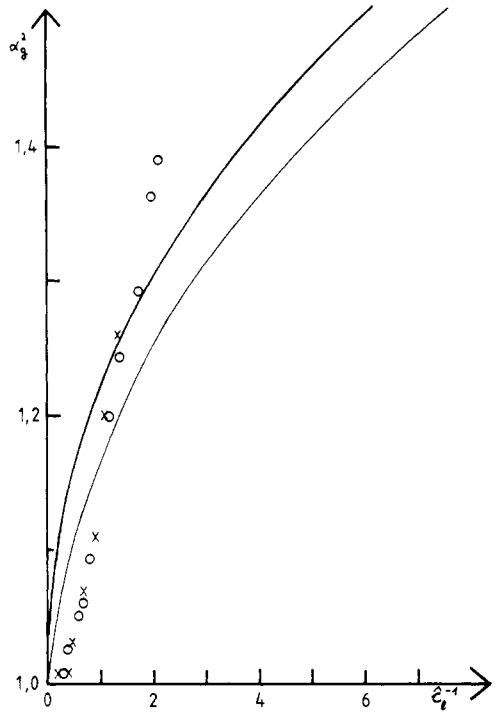

Figure 15. α_g^2 as a function of $\hat{c}_1^{-1}$. The fat curve represents the semidilute limit. The thin curve is calculated for the experimental[18] path in the crossover diagram. Data for PS–cyclohexane: (○) ref 18; (×) ref 39.

mental results of ref 18. We used parameter values Θ = 38 °C as given by the authors and u = 0.6 extracted from results[37] on the osmotic second virial coefficient. The difference of these values compared to those of Table II is a solvent effect since the experiments are run with deuterated cyclohexane. It is obvious that our theory cannot represent these data. Clearly, we have met the semidilute tricritical region (see Figure 3) where the three-body interaction W cannot be neglected. A consistent theory of the crossover into that region is lacking, but we can present a rough analysis[38] inspired by work of Moore.[7] We write

$$\tilde{\xi}_h^{-2}(\tilde{W}) = \tilde{\xi}_h^{-2} + \tilde{W} \tag{5.3}$$

where $\tilde{W}$ is proportional to W. The thin line in Figure 14 represents eq 5.3 with $\tilde{W}$ = 0.5. In view of the roughness of the argument the agreement is satisfactory, in particular if we take into account that neither Θ nor u is fixed very precisely for the deuterated solvent system and that $\tilde{W}$ may be temperature dependent. Basically this explanation is the same as that given in the original paper[18] or in ref 38. It differs in detail because our analysis does not support the view[18] that the excluded volume limit $\xi_h^2 \sim (T - \Theta)^{(4\nu-2)/(3\nu-1)}$ has been reached in the experiment. Also the nonlinear temperature variation of the effective two-body interaction B_1 found in ref 38 cannot be used as an argument against the two-parameter assumption. Whereas ξ_h^2 allows for a decent analysis, the data on R_g^2 pose serious problems. Moore and Al-Noaimi,[8] using an approach essentially equivalent to ours, have shown that these data cannot be explained very well by the temperature crossover scaling function in the semidilute limit. In Figure 15 we have presented this scaling function together with the curve that results if we take the proper experimental path in the crossover diagram Figure 2. Also given are the data of ref 18 and 39. These are obtained from a mixture of few deuterated chains (PSD) in a semidilute solution of normal chains (PSH) in C_6H_{12}. Following ref 37 we in our analysis have used parameter values for PSD–C_6H_{12}: Θ = 30.5 °C, u = 1.8. These values differ strongly from those given in Table II, and it certainly is an open question whether one should use these values or those for PSH–C_6H_{12}. Allowing for a change of Θ and u, we can improve the fit,[8] but it still is not very satisfactory. Furthermore, the optimal value of u is unreasonably large: $u \cong 4$; $\Theta \cong$ 35 °C.

We might hope to improve the situation by including the three-body interaction. Unfortunately, the result for R_g in the Θ-region does not offer a simple heuristic way to include W similar to eq 5.3. Furthermore, the sensitivity to deuteration suggests that an appropriate theoretical approach should allow for different coupling constants f_0 for contacts PSH–PSH, PSD–PSD, or PSH–PSD. Work in that direction is in progress.

6. Conclusions

Not all of the results of this paper are new. In particular, the temperature crossover in the dilute or the semidilute limit has been analyzed before. The new results mainly concern the concentration crossover and its interference with the temperature crossover. What in our view is more important than a specific new result for some special quantity is the fact that here for the first time we have given a unified description of a large variety of observables in the whole critical region. Since for any chemical system there exist at most two nonuniversal parameters, a consistent treatment of all accessible observables greatly increases the predictive power of the theory. Our comparison between theory and experiment reveals an overall agreement that is surprisingly good. In particular, in the region of large overlap the agreement is much better than could be expected on the basis of the large first order corrections.

Clearly, this work should be extended to cover the momentum dependence of the correlation functions for higher q. This can be done only numerically, and the results will be published in a second paper. In view of some large first-order corrections we might also wish to extend the calculations to higher order; this, however, is so tedious that only very restricted results for some special quantities will ever be established, presumably.

Some additional work should also be done on the experimental side. In view of the large scatter and systematic deviations in ψ or α_g^2, it would be desirable to repeat measurements of R_g^2 and A_2^{ls} in order to establish firmly the universal curve. Furthermore, for each measurement of $R_g^2 \equiv \xi^2(c_1 = 0)$ in the dilute limit there certainly exist data on $\xi^2(c_1)$—usually unpublished—which could be used to test our crossover function. This is true in particular for the excluded volume limit. To test the universality of the crossover an extensive measurement similar to that of Chu and Nose, but for some other chemical system, would be welcome. Finally, additional measurements in the semidilute regime seem to be necessary. In particular, it would be of interest to measure ξ^2 in a temperature crossover experiment (light scattering). For longer chains and smaller concentrations than those used in ref 18 we ideally expect to find a region of larger T that is adequately described by our theory, followed by deviations due to tricritical effects as $T \to \Theta$. In that experiment it would be desirable to use some system for which the parameters have been determined in some other region of the crossover diagram.

References and Notes

(1) Yamakawa, H. "Modern Theory of Polymer Solutions"; Harper and Row: New York, 1971.
(2) Edwards, S. F. *Proc. Phys. Soc. London* **1966**, *88*, 265.
(3) Knoll, A.; Schäfer, L.; Witten, T. A. *J. Phys. (Orsay, Fr.)* **1981**, *42*, 767.

(4) Elderfield, D. J. *J. Phys. A: Math. Gen.* **1978**, *11*, 2483; *J. Phys. C: Solid State Phys.* **1980**, *13*, 5883.
(5) des Cloizeaux, J. *J. Phys. (Orsay, Fr.)* **1981**, *42*, 635.
(6) Oono, Y.; Freed, K. F. *J. Phys. A: Math. Gen.* **1982**, *15*, 1931.
(7) Moore, M. A. *J. Phys. (Orsay, Fr.)* **1977**, *38*, 265.
(8) Moore, M. A.; Al-Noaimi, G. F. *J. Phys. (Orsay, Fr.)* **1978**, *39*, 1015.
(9) Elderfield, D. J. *J. Phys. A: Math. Gen.* **1981**, *14*, 3367.
(10) Daoud, M.; Jannink, G. *J. Phys. (Orsay, Fr.)* **1976**, *37*, 973.
(11) Schäfer, L.; Witten, T. A. *J. Phys. (Orsay, Fr.)* **1980**, *41*, 459.
(12) Duplantier, B. *J. Phys. (Orsay, Fr.)* **1982**, *43*, 991.
(13) Brézin, E.; Le Gillou, J. C.; Zinn Justin, J. In "Phase Transitions and Critical Phenomena"; Domb, C., Green, M. S., Eds.; Academic Press: New York, 1976; Vol. 6, p 125.
(14) de Gennes, P.-G. *Phys. Lett. A* **1972**, *38*, 339.
(15) Bruce, A. D.; Wallace, D. J. *J. Phys. A: Math. Gen.* **1976**, *9*, 1117.
(16) de Gennes, P.-G. "Scaling Concepts in Polymer Physics"; Cornell University Press: Ithaca, NY, 1979.
(17) Schäfer, L.; Horner, H. *Z. Phys. B* **1978**, *29*, 251.
(18) Cotton, J. P.; Nierlich, M.; Boué, F.; Daoud, M.; Farnoux, B.; Jannink, G.; Duplessix, R.; Picot, C. *J. Chem. Phys.* **1976**, *65*, 1101.
(19) des Cloizeaux, J. *J. Phys. (Orsay, Fr.)* **1975**, *36*, 281.
(20) Schäfer, L. *Macromolecules* **1982**, *15*, 652.
(21) Bervillier, C. *Phys. Rev. B* **1976**, *14*, 4964.
(22) Witten, T. A.; Schäfer, L. *J. Phys. A: Math. Gen.* **1978**, *11*, 1843.
(23) Cotton, J. P. *J. Phys. Lett. (Orsay, Fr.)* **1980**, *41*, 231.
(24) Miyaki, Y.; Fujita, H. *Macromolecules* **1981**, *14*, 742.
(25) Norisuye, T.; Kawahara, K.; Teramoto, A.; Fujita, H. *J. Chem. Phys.* **1968**, *49*, 4330.
(26) Berry, G. C. *J. Chem. Phys.* **1966**, *44*, 4550.
(27) Yamamoto, A.; Fujii, M.; Tanaka, G.; Yamakawa, H. *Polym. J.* **1971**, *2*, 799.
(28) Fukuda, M.; Fukutomi, M.; Kato, Y.; Hashimoto, T. *J. Polym. Sci., Polym. Phys. Ed.* **1974**, *12*, 871.
(29) Matsumoto, T.; Nishioka, N.; Fujita, H. *J. Polym. Sci., Part A-2* **1972**, *10*, 23.
(30) Kato, T.; Miyaso, K.; Nagasawa, M. *J. Phys. Chem.* **1968**, *72*, 2161.
(31) Miyaki, Y.; Einaga, Y.; Fujita, H. *Macromolecules* **1978**, *11*, 1180.
(32) Noda, I.; Kato, N.; Kitano, T.; Nagasawa, M. *Macromolecules* **1981**, *14*, 668.
(33) Daoud, M.; Cotton, J. P.; Farnoux, B.; Jannink, G.; Sarma, G.; Benoit, H.; Suplessix, R.; Picot, C.; de Gennes, P.-G. *Macromolecules* **1975**, *8*, 804.
(34) Cotton, J. P.; Farnoux, B.; Jannink, G. *J. Chem. Phys.* **1972**, *57*, 290.
(35) Nose, T.; Chu, B. *Macromolecules* **1979**, *12*, 590, 1122; **1980**, *13*, 122.
(36) Schick, M. J.; Doty, P.; Zimm, B. H. *J. Chem. Phys.* **1950**, *72*, 530.
(37) Strazielle, C.; Benoît, H. *Macromolecules* **1975**, *8*, 203.
(38) Okano, K.; Wada, E.; Kurita, K.; Hiramatsu, H.; Fukuro, H. *J. Phys. Lett. (Orsay, Fr.)* **1979**, *40*, 171.
(39) Richards, R. W.; Maconnachie, H.; Allen, G. *Polymer* **1978**, *19*, 266.
(40) Ohta, T.; Oono, Y. *Phys. Lett.* **1982**, *89A*, 460.
(41) Ohta, T.; Nakanishi, A., preprint.
(42) Witten, T. A.; Prentis, J. J. *J. Chem. Phys.* **1982**, *77*, 4247.
(43) Obukhov, S. P. *J. Phys. A: Math. Gen.* **1982**, *15*, L211.
(44) Domb, C.; Barrett, A. J. *Polymer* **1976**, *17*, 179.
(45) Sometimes such an approach is critized because it uses the so-called "$n = 0$ limit".[14] A little thought reveals that this criticism lacks any foundation.[43] Furthermore, all the other RG methods suggested use the same diagrammatic expansion as the "field theoretic" approach. Order for order, these approaches can be transformed into each other by applying some standard (Laplace) transformations.

Evaluation of the Configurational Entropy for Proteins: Application to Molecular Dynamics Simulations of an α-Helix

Ronald M. Levy,*† Martin Karplus,‡ Joseph Kushick,§ and David Perahia∥

Department of Chemistry, Rutgers, The State University of New Jersey, New Brunswick, New Jersey 08903, Department of Chemistry, Harvard University, Cambridge, Massachusetts 02138, Department of Chemistry, Amherst College, Amherst, Massachusetts 01002, and Laboratoire d'Enzymologie Physicochimique et Moleculaire, Universite de Paris-Sud, Orsay, France. *Received July 5, 1983*

ABSTRACT: In this paper we reformulate and extend a method proposed recently for estimating the classical configurational entropy difference between molecular conformations of proteins from molecular dynamics simulations. The method involves a quasi-harmonic oscillator approximation, in which a temperature-dependent (quasi-harmonic) Hamiltonian for the system is parameterized from a detailed computer simulation. The quasi-harmonic potential function is assumed to have a quadratic form with the coefficients chosen so that the mean square fluctuations of the coordinates evaluated from an ensemble average within the harmonic approximation have the same values as the results obtained from a molecular dynamics trajectory on the complete anharmonic potential surface, while the quasi-harmonic kinetic energy function is similar to the standard harmonic expression. It is shown that with the quasi-harmonic Hamiltonian, the effective vibrational frequencies and normal modes can be obtained. This makes possible a detailed comparison with the results obtained from the harmonic approximation and provides a simple procedure for estimating the quantum corrections to thermodynamic properties. The results of vibrational normal mode and molecular dynamics simulations for a polypeptide α-helix are used to calculate the harmonic and quasi-harmonic approximations to the entropy of this model system at three temperatures, 5, 100, and 300 K. The entropy difference ΔS between the two sets of calculations provides an estimate of the importance of anharmonicity in the determination of the configurational entropy.

Introduction

An understanding of the factors that determine the conformational stability and the binding of ligands to proteins requires a thermodynamic analysis. The observed thermodynamic changes in these systems are often the result of a delicate balance between large opposing effects.[1-5] For the analysis of entropy changes associated with different conformational states of proteins it has proved useful to divide the problem into the consideration of (1) hydrophobic effects associated with changes in the ordered state of water molecules and (2) intramolecular "vibrations" associated with changes in the atomic fluctuations of the protein and ligand about mean conforma-

† Rutgers, The State University of New Jersey.
‡ Harvard University.
§ Amherst College.
∥ Universite de Paris-Sud.

0024-9297/84/2217-1370$01.50/0